

1 **Role of Riverine Dissolved Organic and Inorganic**
2 **Carbon and Nutrients in Global-ocean Air-sea CO₂**
3 **Fluxes**

4 **Raphaël Savelli¹, Dustin Carroll^{2,1}, Dimitris Menemenlis¹, Stephanie**
5 **Dutkiewicz^{3,4}, Manfredi Manizza⁵, Anthony Bloom¹, Karel Castro-Morales⁶,**
6 **Charles E. Miller¹, Marc Simard¹, Kevin W. Bowman¹, Hong Zhang¹**

7 ¹Jet Propulsion Laboratory, California Institute of Technology, Pasadena, CA, USA

8 ²Moss Landing Marine Laboratories, San José State University, Moss Landing, CA, USA

9 ³Department of Earth, Atmospheric and Planetary Sciences, Massachusetts Institute of Technology,
10 Cambridge, Massachusetts, USA

11 ⁴Center for Global Change Science, Massachusetts Institute of Technology, Cambridge, Massachusetts,
12 USA

13 ⁵Geosciences Research Division, Scripps Institution of Oceanography, University of California San Diego,
14 La Jolla, California, USA

15 ⁶Institute of Biodiversity, Aquatic Geomicrobiology, Friedrich Schiller University, Jena, Germany

16 **Key Points:**

- 17 • We assess how global lateral exports impact air-sea CO₂ flux and carbon cycling
18 in ECCO-Darwin ocean biogeochemistry simulations
- 19 • Near river mouths, changes in CO₂ flux are dominated by the solubility pump and
20 lead to outgassing
- 21 • Further offshore, riverine nitrogen leads to increased CO₂ uptake via phytoplank-
22 ton fertilization

Corresponding author: Dustin Carroll, dustin.carroll@sjsu.edu

23 Abstract

24 While the preindustrial ocean was assumed to be in equilibrium with the atmosphere,
 25 the modern ocean is a carbon sink, resulting from natural variability and anthropogenic
 26 perturbations, such as fossil fuel emissions and changes in riverine exports over the past
 27 two centuries. Here we use a suite of sensitivity experiments based on the ECCO-Darwin
 28 global-ocean biogeochemistry model to evaluate the response of air-sea CO₂ flux and car-
 29 bon cycling to present-day lateral fluxes of carbon, nitrogen, and silica. We generate a
 30 daily export product by combining point-source freshwater discharge from JRA55-do with
 31 the Global NEWS 2 watershed model, accounting for lateral fluxes from 5171 watersheds
 32 worldwide. From 2000 to 2019, carbon exports increase CO₂ outgassing by 0.22 Pg C
 33 yr⁻¹ via the solubility pump, while nitrogen exports increase the ocean sink by 0.17 Pg
 34 C yr⁻¹ due to phytoplankton fertilization. On regional scales, exports to the Tropical
 35 Atlantic and Arctic Ocean are dominated by organic carbon, which originates from ter-
 36 restrial vegetation and peats and increases CO₂ outgassing (+10 and +20%, respectively).
 37 In contrast, Southeast Asia is dominated by nitrogen from anthropogenic sources, such
 38 as agriculture and pollution, leading to increased CO₂ uptake (+7%). Our results demon-
 39 strate that the magnitude and composition of riverine exports, which are determined in
 40 part from upstream watersheds and anthropogenic perturbations, substantially impact
 41 present-day regional-to-global-ocean carbon cycling. Ultimately, this work stresses that
 42 lateral fluxes must be included in ocean biogeochemistry and Earth System Models to
 43 better constrain the transport of carbon, nutrients, and metals across the land-ocean-
 44 aquatic-continuum.

45 Plain Language Summary

46 Due to ongoing climate change and human activities, the transport of carbon and
 47 nutrients from rivers to the ocean has changed, with rivers now contributing to the mod-
 48 ern ocean’s sequestration of atmospheric carbon dioxide (CO₂). In this study, we add
 49 the effect of present-day rivers to a numerical model of the ocean carbon cycle (ECCO-
 50 Darwin) and then estimate their impact on air-sea CO₂ exchange and ocean biogeochem-
 51 istry. Over a 20-year period, riverine carbon saturates the surface ocean and increases
 52 the amount of CO₂ released to the atmosphere, while nitrogen fertilizes phytoplankton
 53 and increases the capture of atmospheric CO₂ via photosynthesis. In the Tropical At-
 54 lantic and Arctic Oceans, organic carbon drained from vegetation and peats causes out-
 55 gassing of ocean carbon. In Southeast Asia, the large amount of riverine nitrogen orig-
 56 inating from human activities, such as agriculture or waste water, increases ocean CO₂
 57 sequestration. Our work highlights how rivers, which are affected by present-day human
 58 actions and climate change, impacts the ocean’s carbon cycle across regional-to-global
 59 scales.

60 1 Introduction

61 Globally, shelf and marginal seas are typically sinks of CO₂, where uptake driven
 62 by strong biological productivity exceeds outgassing from organic matter degradation
 63 and carbon enrichment by river runoff and coastal upwelling (Ianson et al., 2009; W.-
 64 J. Cai, 2011; W. Cai et al., 2013; Laruelle et al., 2017; Bertin et al., 2023). Rivers trans-
 65 port roughly 0.8–0.9 Pg C yr⁻¹ from land to coastal regions as dissolved organic carbon
 66 (DOC), dissolved inorganic carbon (DIC), particulate organic carbon (POC), and partic-
 67 ulate inorganic carbon (PIC); a third of the aforementioned total riverine export of
 68 carbon is buried in coastal sediments (Regnier et al., 2022; Battin et al., 2023). Nutri-
 69 ents such as phosphorus, nitrogen, and silica are also conveyed by rivers along with car-
 70 bon. Terrestrial inorganic carbon and nutrients in streams originate from weathering of
 71 the lithosphere and the associated sink of atmospheric CO₂, along with the remineral-
 72 ization of organic matter in streams and/or on land (Suchet & Probst, 1995; Battin et

73 al., 2023). Riverine organic carbon and nutrients are further supplemented by primary
74 production from land vegetation and organic matter mobilized through direct litterfall,
75 runoff, leaching, and erosion into rivers (Meybeck & Vörösmarty, 1999; Seitzinger et al.,
76 2010; Regnier et al., 2013; Battin et al., 2023).

77 Once injected into the coastal ocean, riverine carbon is generally outgassed back
78 to the atmosphere in the form of CO₂, due to the saturation of surface-ocean waters by
79 terrestrial DIC and remineralization of terrestrial organic matter (Hartmann et al., 2009;
80 Lacroix et al., 2020; Bertin et al., 2023) in shallow, well-mixed water columns. The nat-
81 ural transport of carbon from terrestrial ecosystems to ocean outgassing, the so-called
82 “river loop”, is estimated to be 0.65 ± 0.3 Pg C yr⁻¹ (Regnier et al., 2022; Friedlingstein
83 et al., 2023). With respect to inorganic nutrients, their injection into the surface ocean
84 can fertilize growth of photosynthetic organisms in nutrient-limited regions. Globally,
85 this lateral flux increases ocean primary productivity and contributes to a coastal-ocean
86 sink of ~ 0.25 Pg C yr⁻¹, which is roughly 17% of the global-ocean sink (W.-J. Cai, 2011;
87 Lacroix et al., 2021; S. Gao et al., 2023).

88 Over the past two centuries, terrestrial anthropogenic perturbations have led to a
89 substantial increase in the load of nitrogen and phosphorus through agricultural fertil-
90 ization, leaked sewage, and land-use change (Smith et al., 2003; Lee et al., 2016; Lacroix
91 et al., 2021). Projections of the historical riverine dissolved nitrogen and phosphorus load
92 depict a three- to four-fold increase over the period 1900–2019 (Lacroix et al., 2021). When
93 delivered in excessive amounts, these nutrients can alter aquatic and ocean ecosystems,
94 resulting in eutrophication, hypoxia, and acidification in coastal waters (Laurent et al.,
95 2017; Fennel & Testa, 2019). Dissolved and particulate carbon are also affected region-
96 ally by agricultural liming, the addition of sulfuric acid to watersheds, changes in ero-
97 sion patterns, and river management (Monteith et al., 2007; Raymond et al., 2008; Calmels
98 et al., 2007; Regnier et al., 2013; Maavara et al., 2017). Projected trends for river bio-
99 geochemical loads remain uncertain and exhibit disparate regional responses over the 21st
100 century depending on the chosen shared socioeconomic pathway (Beusen et al., 2022; Beusen
101 & Bouwman, 2022; Vishwakarma et al., 2022; Zhang et al., 2022).

102 While present estimates of riverine freshwater and biogeochemical fluxes are poorly
103 sampled in space and time, land surface and watershed models can provide spatiotemporally-
104 resolved lateral exports at global scales (Mayorga et al., 2010; Krinner et al., 2005; Hage-
105 mann & Dümenil, 1997; Hagemann & Gates, 2003; M. Li et al., 2017; Bloom et al., 2020).
106 Coupled with ocean biogeochemical models, it is thus possible to quantify the response
107 of the coastal and open-ocean carbon cycle to lateral fluxes (Lacroix et al., 2020, 2021;
108 Mathis et al., 2022; Louchard et al., 2021; da Cunha & Buitenhuis, 2013; Le Fouest et
109 al., 2013; S. Gao et al., 2023; Bertin et al., 2023). Regarding the importance of lateral
110 exports in ocean carbon cycling, it is critical that ocean biogeochemical models better
111 account for coastal mechanisms occurring across the land-ocean-aquatic-continuum (LOAC)
112 (Ward et al., 2020; Mathis et al., 2022). Such improvements will come from 1) finer hor-
113 izontal and vertical grid resolution to resolve small-scale ocean physics (vertical mixing,
114 submesoscale processes) and associated biology (hypoxia, phytoplankton blooms) and
115 2) improved representation of LOAC components (river and groundwater discharge, bot-
116 tom sediment diagenesis, and estuarine biogeochemical filtering) (Ward et al., 2020; Sharples
117 et al., 2017). While recent modeling efforts have made improvements in this regard (Volta
118 et al., 2016; Laruelle et al., 2017; Mathis et al., 2022, 2024), the respective contribution
119 of riverine exports to air-sea CO₂ fluxes across the global ocean remains to be assessed.

120 In this study, we add lateral fluxes of carbon and nutrients to the ECCO-Darwin
121 global-ocean biogeochemistry state estimate (Carroll et al., 2020, 2022) and evaluate the
122 response of air-sea CO₂ flux and ocean biogeochemistry to daily point-source river forc-
123 ing from 2000–2019. We compute daily riverine biogeochemical export by combining point-
124 source freshwater discharge from the JRA55-do atmospheric reanalysis with the Global
125 NEWS 2 watershed model (Mayorga et al., 2010; Suzuki et al., 2018; Tsujino et al., 2018;

126 Feng et al., 2021). We then investigate the respective contribution of dissolved organic
 127 and inorganic carbon, nitrogen, and silica to air-sea CO₂ fluxes at coastal, basin, and
 128 global scales, as performed in Lacroix et al. (2020). This paper provides new tools and
 129 methods for improved estimates of how riverine biogeochemical exports impact ocean
 130 carbon cycling, which is pivotal for understanding the response of ocean biogeochemistry
 131 to anthropogenic perturbations on land.

132 2 Methods

133 2.1 The ECCO-Darwin Ocean Biogeochemistry State Estimate

134 The ECCO-Darwin ocean biogeochemistry state estimate is extensively described
 135 in Brix et al. (2015), Manizza et al. (2019) and Carroll et al. (2020, 2022, 2024). For the
 136 ECCO-Darwin solution presented in this paper, ocean physics (circulation, temperature,
 137 salinity, and sea ice) are provided by the Estimating the Circulation and Climate of the
 138 Ocean (ECCO) global-ocean and sea-ice data synthesis version 4 release 5 (V4r5) (For-
 139 get et al., 2015).

140 The horizontal grid is based on the LLC90 (Lat-Lon-Cap 90) grid, which is described
 141 in detail in (Forget et al., 2015). The nominal horizontal grid resolution in ECCO v4 LLC90
 142 is 1° (~55 km at high latitudes). The vertical discretization consists of 50 z-levels, rang-
 143 ing from 10-m thickness in the top 7 levels to 450 m at depth. ECCO v4 uses a third-
 144 order, direct-space-time tracer advection scheme in the horizontal and an implicit third-
 145 order upwind scheme in the vertical; a time step of 3600 s is used. Vertical mixing is pa-
 146 rameterized using the Gaspar–Grégoris–Lefevre (GGL) mixing-layer turbulence closure
 147 and convective adjustment scheme (Gaspar et al., 1990). ECCO v4 assimilates physi-
 148 cal observations via the 4-D adjoint method (Wunsch et al., 2009; Wunsch & Heimbach,
 149 2013).

150 Daily river runoff in the present configuration is based on the Japanese 55-year at-
 151 mospheric reanalysis (JRA55-do) river forcing dataset, which uses the CaMa-Flood global
 152 river routing model and adjusted runoff from the land component of JRA-55 (Suzuki et
 153 al., 2018; Tsujino et al., 2018; Feng et al., 2021). Point source JRA55-do freshwater runoff
 154 (m s⁻¹) was added to ECCO v4 as a real freshwater flux in the surface ocean (first ver-
 155 tical level) at the closest ECCO v4 LLC90 grid cell along the coastal periphery. The fresh-
 156 water flux was adjusted according to the difference in grid cell area between JRA55-do
 157 (0.25°x 0.25°) and ECCO v4 LLC90. A full evaluation of ocean physics from ECCO v4
 158 LLC90 compared to observations can be found in the Supporting Information and Feng
 159 et al. (2021).

160 ECCO v4 LLC90 ocean physics was coupled online with the Massachusetts Insti-
 161 tute of Technology Darwin Project ecosystem model described in Brix et al. (2015). The
 162 ecosystem model solves 39 prognostic variables such as carbon, nitrogen, phosphorus,
 163 iron, silica, oxygen, and alkalinity. The model simulates their respective cycle from in-
 164 organic pools to living/dead matter of plankton organisms and the subsequent reminer-
 165 alization, all driven by the ocean physics. The carbonate chemistry is solved by the method
 166 in Follows et al. (2006). Plankton species consist of five large-to-small functional phy-
 167 toplankton types (diatoms, other large eukaryotes, *Synechococcus*, and low- and high-
 168 light adapted *Prochlorococcus*), and two zooplankton types. Atmospheric CO₂ partial
 169 pressure at sea level (apCO₂) from the National Oceanic and Atmospheric Administra-
 170 tion Marine Boundary Layer Reference product (Andrews et al., 2014) was used to drive
 171 air-sea CO₂ fluxes computed by the model according to Wanninkhof (1992). Atmospheric
 172 iron dust is deposited at the ocean surface based on the monthly climatology of Mahowald
 173 et al. (2009). Once at the ocean bottom, particulate inorganic and organic matter is re-
 174 moved at the sinking rate to limit the accumulation of particulates on the seafloor. Bio-
 175 geochemical observations were used to optimize the biogeochemical model using a Green’s

176 Functions approach (Menemenlis et al., 2005); the optimization methodology and asso-
177 ciated data are fully described in Carroll et al. (2020). The ECCO-Darwin solution was
178 previously published using monthly climatological freshwater runoff forcing from Fekete
179 et al. (2002). Here, the Baseline simulation consists of the same ocean biogeochemistry
180 simulation as Carroll et al. (2020), but with daily point-source freshwater runoff from
181 January 1992 to December 2019. To allow partial adjustment to these new boundary con-
182 ditions, the analysis period hereinbelow spans the last 20 years of the simulation, Jan-
183 uary 2000 to December 2019. Figure 1 shows the general match-up between time-mean
184 ECCO-Darwin air-sea CO₂ fluxes and the MPI SOM FFN v2022 (Landschützer et al.,
185 2016; Jersild et al., 2023) and Jena CarboScope v2023 (Rödenbeck et al., 2013) prod-
186 ucts for the 2000–2019 study period.

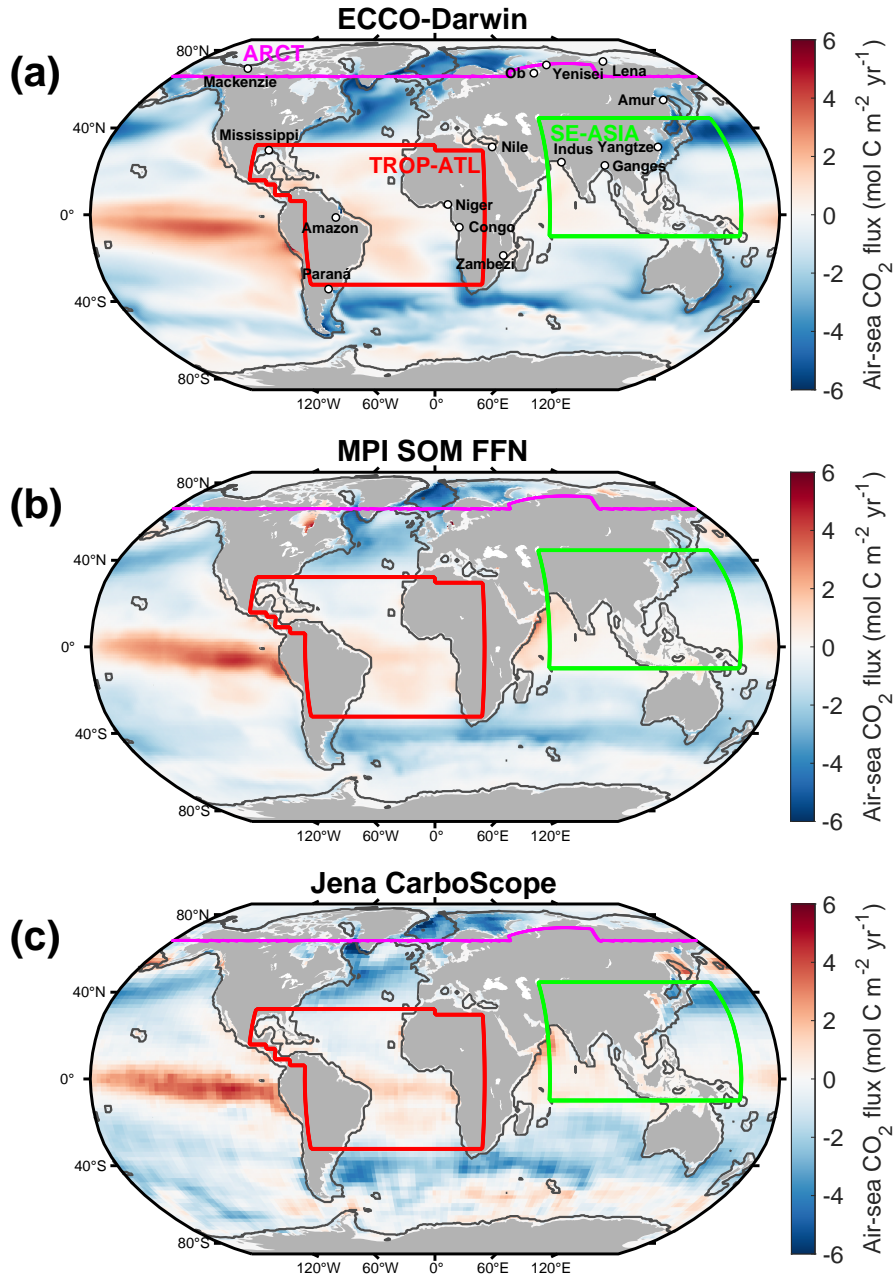


Figure 1. Climatological global-ocean air-sea CO₂ flux for (a) ECCO-Darwin Baseline, (b) MPI SOM FFN, and (c) Jena CarboScope. Positive values represent CO₂ outgassing (red colors); negative values are uptake (blue colors). All fields shown are time means from January 2000 to December 2019. Colored boundary lines correspond to domains used for regional analysis of the Arctic Ocean (ARCT, violet line), the Tropical Atlantic (TROP-ATL, red line), and Southeast Asia (SE-ASIA, green line). The black line delineates the coastal ocean from the open ocean, which is set by the furthest point from the coastline of either a 300-km distance or the 1000-m isobath. White points show river mouth locations for the top-15 global rivers in terms of watershed area. MPI SOM FFN v2022 and Jena CarboScope v2023 products were interpolated on the ECCO v4 LLC90 grid.

2.2 Biogeochemical River Runoff

In addition to the Baseline simulation, we conducted a suite of sensitivity experiments where we added terrestrial DOC (t_{DOC}), DIC (t_{DIC}), total alkalinity (t_{ALK}), dissolved inorganic nitrogen (t_{DIN}), dissolved organic nitrogen (t_{DON}), and dissolved silica (t_{DSi}), henceforth referred to as riverine exports in this study. We excluded phosphorus and iron due to the complexity of their reactions when entering the marine environment (i.e., absorption, bio-availability). Except for t_{DIC} and t_{ALK} , riverine exports are provided by the Global NEWS 2 (Global Nutrient Export from WaterSheds) model (Mayorga et al., 2010).

Global NEWS 2 uses statistical and mechanistic relations at the watershed scale to compute annual-mean freshwater discharge and riverine loads based on natural and anthropogenic sources, with 6292 individual watersheds delineated according to the global river systems dataset from Vörösmarty et al. (2000). t_{DIN} was partitioned into nitrite (NO_2^-), nitrate (NO_3^-), and ammonium (NH_4^+), according to the mean fraction of each species concentration relative to the total DIN concentration from the GLOBAL RIVER CHEMISTRY Database (GLORICH) (Hartmann et al., 2014). The NO_2^- :DIN, NO_3^- :DIN, and NH_4^+ :DIN ratios were estimated to be 0.02, 0.65, and 0.33, respectively. Riverine t_{DIC} loads were computed using an empirical relation between freshwater discharge and gross CO_2 consumption from rock weathering as described in M. Li et al. (2017, equation 9). CO_2 consumption by rock weathering over each Global NEWS 2 watershed was estimated based on the freshwater discharge and the basin-dominant lithology (Amiotte Suchet et al., 2003). t_{ALK} loads were computed using an ALK:DIC ratio (0.98) based on the mean total ALK compared to DIC from GLORICH. t_{DOC} was not considered to be more refractory than marine DOC; the DOC remineralization rate is set to 1 over 100 days. We used Global NEWS 2 outputs for year 2000 as representative of present-day carbon and nutrient loads (Mayorga et al., 2010).

Global NEWS 2 river mouth locations were associated with JRA55-do grid points exhibiting the closest annual-mean freshwater discharge in 2000 within a euclidean distance of 5° . The top-100 largest rivers (by watershed extent) from Global NEWS 2 were imposed on JRA55-do grid points as a function of distance only. In total, 5171 river mouths were associated with JRA55-do grid points. For each discharge point, export concentrations from the associated river were estimated by dividing the load by the annual volume of freshwater from Global NEWS 2; the concentration was then converted to a daily flux using the corresponding daily-mean freshwater flux from JRA55-do. Exports were adjusted according to the grid cell area difference between JRA55-do and ECCO v4 LLC90. These biogeochemical exports were then added as point-source discharge along riverine freshwater flux (Figure 2). Due to extreme values in our automated Global-NEWS-2-derived computation for the Amazon River, the DIC load for this system was set to a more-realistic, literature-mean of $2.54 \text{ Tmol yr}^{-1}$ (da Cunha & Buitenhuis, 2013; Probst et al., 1994; M. Li et al., 2017) (for more details see Supporting Information Text S1).

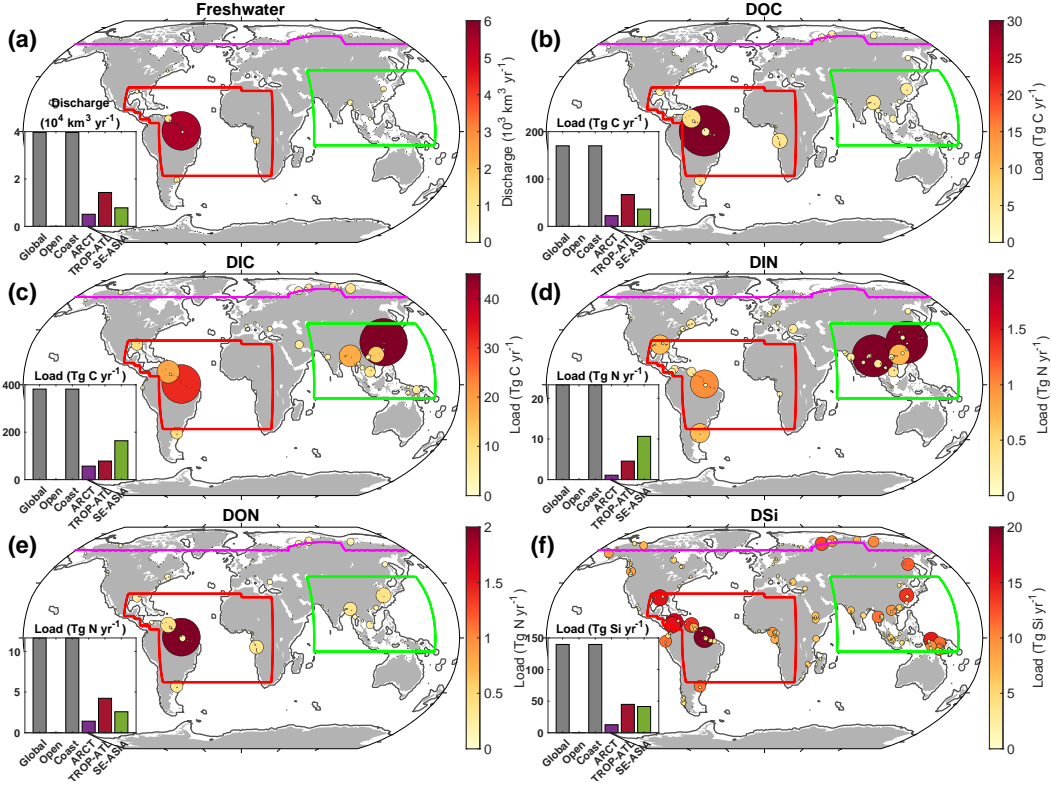


Figure 2. Riverine freshwater discharge and biogeochemical exports resulting from the association of Global NEWS 2 and JRA55-do on the ECCO v4 LLC90 grid. Domain-scale freshwater discharge and load is relative to the respective domain area. Insets show corresponding year-2000 discharge/load for various regions. The size of circles represents magnitude of loads. Colored boundaries correspond to domains used for regional analysis. The black line delineates the coastal ocean from the open ocean. Only rivers with annual discharge over $10 \text{ km}^3 \text{ yr}^{-1}$ are shown.

227 As riverine t_{DOC} , t_{DIN} , t_{DON} , and t_{DSi} were computed from Global NEWS 2 con-
 228 centration and modulated with JRA55-do freshwater runoff, our fluxes agree well with
 229 existing estimates based on the NEWS 2 database (Mayorga et al., 2010; Frings et al.,
 230 2016; Sharples et al., 2017; Lacroix et al., 2020; Tivig et al., 2021; Tian et al., 2023). t_{DIC}
 231 lateral export from rivers was estimated according to Amiotte Suchet et al. (2003); May-
 232 orga et al. (2010); M. Li et al. (2017), resulting in a t_{DIC} load of $381.81 \text{ Tg C yr}^{-1}$ to
 233 the ocean, which is in general agreement with recent studies (Drake et al., 2018; M. Li
 234 et al., 2017; Lacroix et al., 2020; Battin et al., 2023; Tian et al., 2023).

2.3 Sensitivity Experiments and Analysis

235
 236 Sensitivity experiments consisted of adding riverine exports separately or together
 237 along with freshwater runoff (Table 1). t_{ALK} was always added along with t_{DIC} in rel-
 238 evant experiments. Moreover, we ran additional sensitivity experiments using all river-
 239 ine exports (Table 1, ALL_{run}) for each of the top-15 global rivers in terms of watersheds
 240 extent (Mayorga et al., 2010). Ancient river systems and rivers terminating in enclosed
 241 basins or on land were discarded from our analysis. The locations of the corresponding
 242 top-15 river mouths are shown in Figure 1.

Table 1. Annual carbon and nutrient loads in runoff sensitivity experiments.

Experiment Name	t_{DOC} (Tg C yr ⁻¹)	t_{DIC} (Tg C yr ⁻¹)	t_{DON} (Tg N yr ⁻¹)	t_{DIN} (Tg N yr ⁻¹)	t_{DSi} (Tg Si yr ⁻¹)
Baseline	0	0	0	0	0
DC _{run}	170.1	381.8	0	0	0
DIC _{run}	0	381.8	0	0	0
DN _{run}	0	0	11.7	23.3	0
DIN _{run}	0	0	0	23.3	0
DSi _{run}	0	0	0	0	139.7
ALL _{run}	170.1	381.8	11.7	23.3	139.7

243 We analyzed monthly-mean model fields along the coastal ocean (limits set by the
 244 furthest point from the coastline, either the 1000-m isobath or a distance of 300 km; 58
 245 x 10⁶ km²) and the open ocean (300 x 10⁶ km²) during 2000–2019. In addition to the
 246 global ocean, we also evaluated the sensitivity of ocean carbon cycling in three specific
 247 regions that receive large volumes of freshwater from major river systems: the Arctic Ocean
 248 (ARCT, 22 x 10⁶ km²), Tropical Atlantic (TROP-ATL, 77 x 10⁶ km²), and Southeast
 249 Asia (SE-ASIA, 62 x 10⁶ km²). Coastal and open ocean boundaries are delineated by
 250 the black line in Figure 1. Monthly-mean net primary production (NPP) was integrated
 251 over the upper 100 m.

252 Furthermore, we separated the respective contributions of 1) the solubility pump
 253 and 2) primary production resulting from river-driven changes in climatological air-sea
 254 CO₂ flux (ΔCO_2) in the ALL_{run} as:

$$\Delta\text{CO}_2_{ALL_{run}} = \Delta\text{CO}_2^{\text{solub}^C} + \Delta\text{CO}_2^{\text{solub}^{N,Si}} + \Delta\text{CO}_2^{\text{NPP}^{N,Si}}, \quad (1)$$

255 where $\Delta\text{CO}_2^{\text{solub}^C}$ and $\Delta\text{CO}_2^{\text{solub}^{N,Si}}$ are the changes in air-sea CO₂ flux associated
 256 with the solubility pump due to the addition of terrestrial carbon and nitrogen/silica,
 257 respectively. $\Delta\text{CO}_2^{\text{NPP}^{N,Si}}$ is the change in air-sea CO₂ flux driven by NPP in response
 258 to terrestrial nitrogen and silica.

259 In DC_{run}, changes in air-sea CO₂ flux are only associated with the solubility pump:

$$\Delta\text{CO}_2^{\text{solub}^C} = \Delta\text{CO}_2_{DC_{run}}. \quad (2)$$

260 We then associated the change in surface-ocean DIC concentration with ΔCO_2 driven
 261 by the solubility pump in DC_{run} to isolate ΔCO_2 due to the solubility pump relative to
 262 changes in surface-ocean DIC concentration in DN and DSi_{runs}:

$$\Delta\text{CO}_2^{\text{solub}^{N,Si}} = \frac{\Delta\text{CO}_2^{\text{solub}^C}}{[DIC]_{surf}^C} \times [DIC]_{surf}^{N,Si}. \quad (3)$$

263 The change in ΔCO_2 due to changes in NPP in DN and DSi_{runs} was then estimated
 264 by subtracting ΔCO_2 due to the solubility pump from the total ΔCO_2 :

$$\Delta\text{CO}_2^{\text{NPP}^{N,Si}} = \Delta\text{CO}_2_{DN,DSi_{runs}} - \Delta\text{CO}_2^{\text{solub}^{N,Si}}. \quad (4)$$

3 Results

3.1 Climatological Global Analysis

Along with $39,687 \text{ km}^3 \text{ yr}^{-1}$ of riverine freshwater, total loads of $551.9 \text{ Tg C yr}^{-1}$, 35 Tg N yr^{-1} , and $139.7 \text{ Tg Si yr}^{-1}$ were exported into the global ocean in ALL_{run} (Table 1). The addition of dissolved carbon, nitrogen, and silica in ALL_{run} led to an increase in CO_2 outgassing of $0.03 \text{ Pg C yr}^{-1}$ compared to the Baseline, globally (Figure 3a and Figure 4a, Table 2). The majority of CO_2 outgassing ($0.04 \text{ Pg C yr}^{-1}$) occurs in the coastal ocean (Figure 3a and Table 2). In the open ocean, riverine exports slightly increased CO_2 uptake by $0.01 \text{ Pg C yr}^{-1}$ (Figure 3a and Table 2).

In ALL_{run} , changes in air-sea CO_2 flux resulted from compensation between the effects of riverine carbon and nitrogen, as DC_{run} and DN_{run} experiments result in elevated CO_2 outgassing and uptake, respectively (Table 2). In DC_{run} , the increase in ocean carbon due to riverine exports diminished the ocean's capacity to take up atmospheric CO_2 , resulting in a net CO_2 outgassing of $0.22 \text{ Pg C yr}^{-1}$ (Table 2). In DN_{run} , the increase in nutrients to the euphotic zone led to increased phytoplankton productivity. The additional uptake of carbon by phytoplankton decreased surface-ocean DIC, resulting in an additional CO_2 sink of $0.17 \text{ Pg C yr}^{-1}$ (Table 2).

CO_2 outgassing driven by riverine carbon (DC_{run}) was dominated by t_{DOC} (70%), with a smaller contribution from t_{DIC} (30%) (Figure 4a). While outgassing driven by riverine carbon was compensated by uptake due to nitrogen in the open ocean, CO_2 uptake due to nitrogen was 36% lower than riverine-carbon-driven coastal outgassing, leading to global-ocean net CO_2 outgassing in ALL_{run} (Table 2).

Riverine dissolved carbon, nitrogen, and silica also resulted in a NPP increase of 0.6 Pg C yr^{-1} (+2%) compared to Baseline (Figure 3b and Figure 4b, Table 2). Riverine t_{DIN} (DIN_{run}) contributed to 70% and 86% of the CO_2 uptake and NPP increase simulated in DN_{run} , respectively (Figure 4b). The total increase of NPP in ALL_{run} from riverine exports was equally distributed between the coastal and open ocean (0.3 Pg C yr^{-1} for each) (Figure 4b). However, the increase of NPP was stronger in the coastal ocean ($+5.2 \text{ g C m}^{-2} \text{ yr}^{-1}$, +7%) compared to the open ocean ($+1 \text{ g C m}^{-2} \text{ yr}^{-1}$, +1%) relative to their surface area.

Table 2. Air-sea CO₂ flux and NPP for each experiment in the coastal ocean, open ocean, and global ocean. Positive values represent CO₂ outgassing; negative values are uptake.

Domain	Experiment	CO ₂ Flux (Pg C yr ⁻¹)	NPP (Pg C yr ⁻¹)
Coastal Ocean			
	Baseline	-0.68	3.8
	ALL _{run} - Baseline	+0.04	+0.3
	DC _{run} - Baseline	+0.1	0.0
	DN _{run} - Baseline	-0.07	+0.3
	DSi _{run} - Baseline	-0.01	+0.01
Open Ocean			
	Baseline	-1.90	20.6
	ALL _{run} - Baseline	-0.01	+0.3
	DC _{run} - Baseline	+0.1	0.0
	DN _{run} - Baseline	-0.1	+0.3
	DSi _{run} - Baseline	-0.01	+0.01
Global Ocean			
	Baseline	-2.58	24.4
	ALL _{run} - Baseline	+0.03	+0.6
	DC _{run} - Baseline	+0.22	0.0
	DN _{run} - Baseline	-0.17	+0.6
	DSi _{run} - Baseline	-0.01	+0.01

3.2 Climatological Regional Analysis

The Arctic Ocean region (Figure 1, ARCT) received 5,138 km³ yr⁻¹ of freshwater from rivers in Baseline, which is roughly 13% of global freshwater discharge. In ALL_{run}, freshwater discharge was supplemented with 22.6 and 56.8 Tg C yr⁻¹ of t_{DOC} and t_{DIC}, respectively (Figure 2). The river load of carbon and t_{DOC} into ARCT represented 15% and 12% of their associated global loads, respectively. ARCT also received 2.5 Tg N yr⁻¹ as t_{DON} (56%) and t_{DIN} (44%) in ALL_{run}. The t_{DSi} river load was 12.6 Tg Si yr⁻¹ (Figure 2) in this region. Riverine export loads were primarily from the Ob, Yenisei, Lena, and Mackenzie Rivers (Figure 2 and Supporting Information Table S1).

In Baseline, ARCT produced a CO₂ uptake of roughly 0.21 Pg C yr⁻¹. When riverine carbon, nitrogen, and silica were added in ALL_{run}, ARCT CO₂ uptake was reduced by 0.02 Pg C yr⁻¹, with the majority of the response (80%) in the coastal ocean (Figure 3a and Figure 4a). Riverine-induced CO₂ outgassing was dominated by the input of t_{DOC} in ARCT (Figure 4a). 50% of the riverine-induced CO₂ outgassing was due to the Ob, Yenisei, Lena, and Mackenzie Rivers (Table 3). In the Baseline experiment, NPP was 0.22 Pg C yr⁻¹, with a similar magnitude in the coastal and open ocean. The addition of riverine nitrogen into ARCT increased coastal NPP by 40% (Figure 3b and Figure 4b).

The Tropical Atlantic (Figure 1, TROP-ATL) received 36% of global freshwater discharge (14,228 km³ yr⁻¹) and 35% of the global t_{DOC} load from rivers (67.2 Tg C yr⁻¹). Combined with t_{DIC}, the net carbon load was 145.3 Tg C yr⁻¹ (Figure 2). Roughly 30% of the global dissolved nitrogen and silica river load was delivered to TROP-ATL, with river loads dominated by the Amazon River (Figure 2 and Supporting Information Table S1).

319 Riverine carbon, nitrogen, and silica resulted in a TROP-ATL CO₂ outgassing of
 320 0.02 Pg C yr⁻¹ compared to Baseline (0.10 Pg C yr⁻¹). This imbalance resulted from
 321 CO₂ outgassing driven by carbon, which was 30% larger than uptake due to increased
 322 phytoplankton productivity from riverine nitrogen (Figure 4a). 85% of CO₂ outgassing
 323 in DC_{run} was driven by riverine t_{DOC} (Figure 4a). Riverine t_{DOC} indirectly drives CO₂
 324 outgassing by first being remineralized to DIC, which increases DIC concentration in the
 325 ocean and thus limits the ocean’s capacity to take up atmospheric CO₂. Most of the CO₂
 326 outgassing driven by t_{DOC} occurs in the open ocean (Figure 3a and Figure 4a). The Ama-
 327 zon River drove 70% of riverine-induced CO₂ outgassing in TROP-ATL (Table 3). In
 328 Baseline, NPP in TROP-ATL was 3.18 Pg C yr⁻¹. The increase in NPP driven by river-
 329 ine t_{DIN} occurred predominantly in the open ocean (~60%) compared to the coastal (~40%)
 330 zone (Figure 4b). The Amazon River was responsible for 65% of the NPP increase driven
 331 by riverine exports (Figure 4b).

332 In Baseline, the freshwater discharge into SE-ASIA was 7,841 km³ yr⁻¹, roughly
 333 20% of global discharge. In ALL_{run}, SE-ASIA received 38% of dissolved carbon from rivers,
 334 globally (207.39 Tg C yr⁻¹). 81% of dissolved carbon delivered into SE-ASIA was in-
 335 organic, representing 42% of the global t_{DIC} river load (Figure 2). SE-ASIA also received
 336 45% (10.6 Tg N yr⁻¹) of the global t_{DIN} load from rivers (Figure 2). 41.5 Tg Si yr⁻¹
 337 was discharged into SE-ASIA (Figure 2). Nutrient loads into SE-ASIA were dominated
 338 by high riverine t_{DIC} and t_{DIN} from the Ganges and Yangtze Rivers (Figure 2 and Sup-
 339 porting Information Table S1). The Yangtze river contributed 12% of t_{DIC} river loads,
 340 globally (Figure 2 and Supporting Information Table S1). Taken together, the Yangtze
 341 and Ganges Rivers delivered 20% of the global t_{DIN} river load (Figure 2 and Support-
 342 ing Information Table S1).

343 SE-ASIA had a CO₂ sink of 0.30 Pg C yr⁻¹ in Baseline, while CO₂ uptake increased
 344 by 0.02 Pg C yr⁻¹ in ALL_{run} (Figure 4a). Riverine carbon- and nitrogen-driven air-sea
 345 CO₂ flux was compensated in the coastal ocean (±0.03 Pg C yr⁻¹). However, in the open
 346 ocean, the riverine nitrogen-driven increase in NPP and associated CO₂ uptake was two
 347 times higher than carbon-driven outgassing — leading to an overall imbalance and re-
 348 sulting in net CO₂ uptake in the domain (Figure 4a).

349 t_{DIN} was responsible for 85% of biological CO₂ uptake (Figure 4a). The Ganges
 350 River (58%), combined with the Indus and Yangtze Rivers, were responsible for 77% of
 351 CO₂ uptake in SE-ASIA (Table 3). NPP in SE-ASIA without the addition of riverine
 352 exports was 3.3 Pg C yr⁻¹. In ALL_{run}, NPP increased by 0.30 Pg C yr⁻¹ due to ele-
 353 vated t_{DIN} in both the open and coastal ocean (Figure 4b). The Ganges and Yangtze
 354 Rivers caused roughly 40% of the NPP increase in SE-ASIA (Table 3).

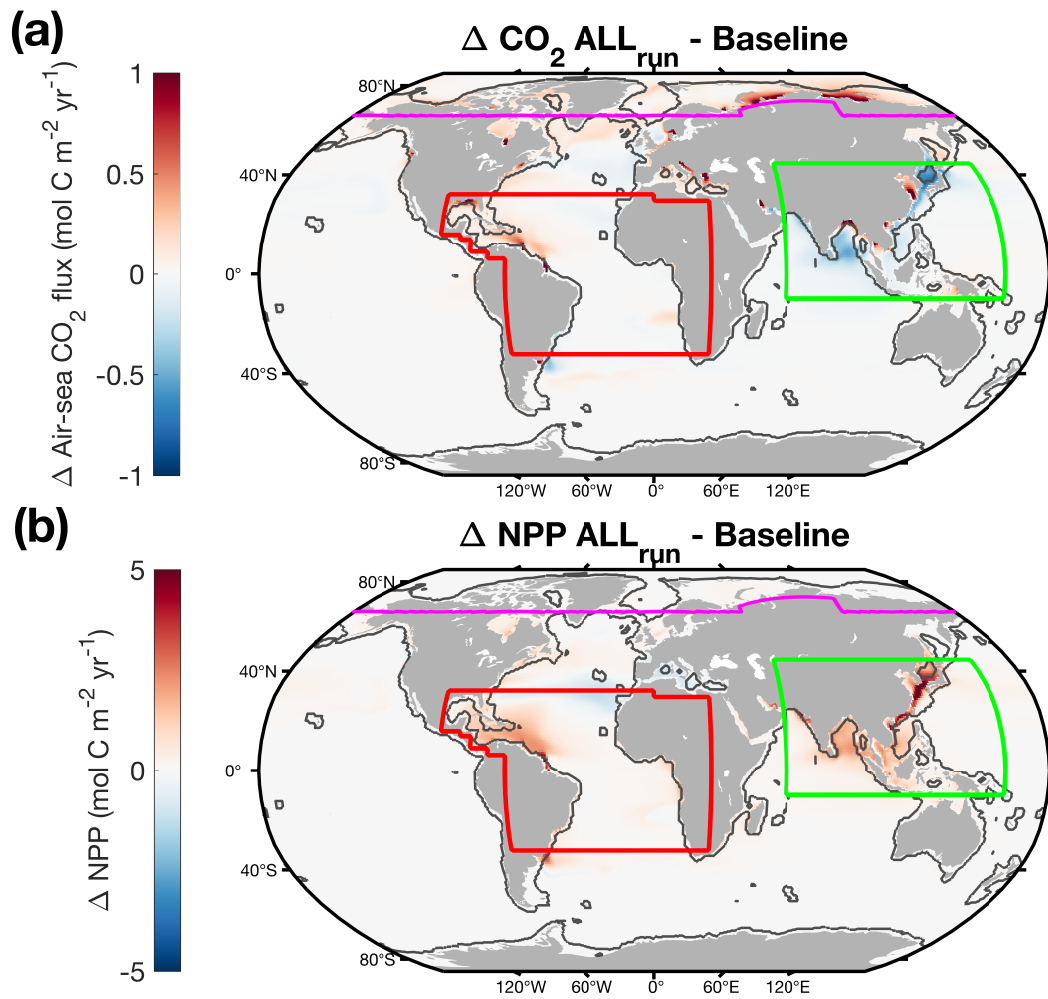


Figure 3. Global-ocean (a) air-sea CO_2 flux and (b) NPP driven by riverine exports in ALL_{run} . Fields represent time-mean values from January 2000 to December 2019. Colored lines on maps show domains used for regional analysis. The black line delineates the coastal ocean from the open ocean.

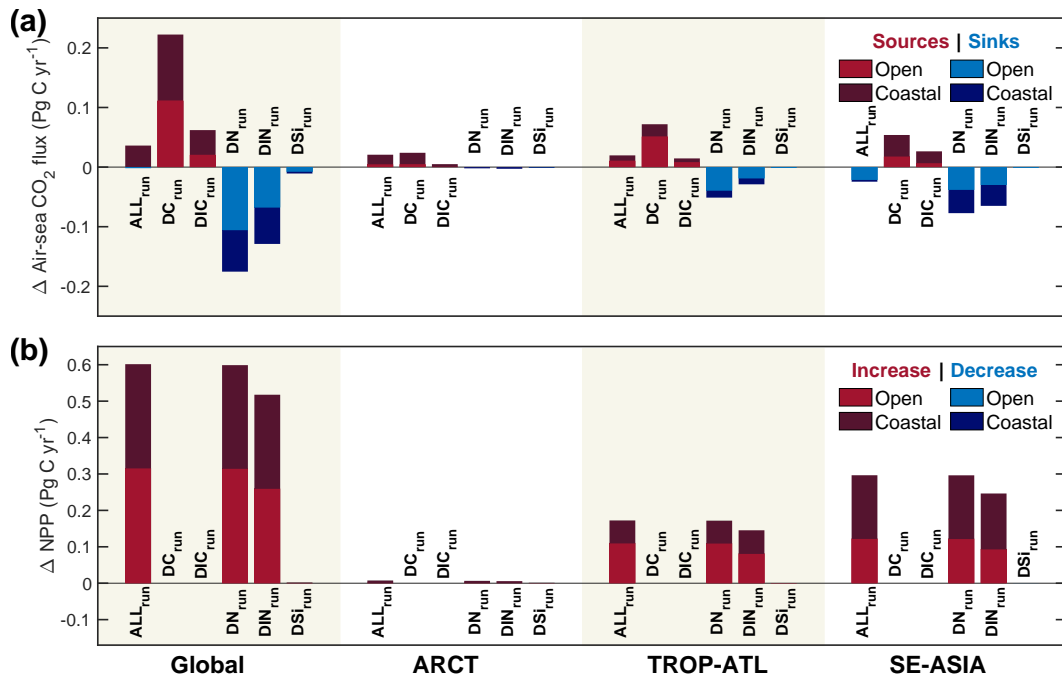


Figure 4. Domain-integrated differences in (a) air-sea CO_2 flux and (b) NPP driven by riverine exports in each sensitivity experiment. Differences were computed from time-mean fields from January 2000 to December 2019. The black line delineates the coastal ocean from the open ocean.

Table 3. Contribution of the global top-15 rivers in terms of watershed area to changes in air-sea CO₂ flux and NPP. Positive values represent CO₂ outgassing driven by the corresponding river; negative values are uptake. The respective river contribution is estimated from the difference between Baseline and a modified ALL_{run}, where only the corresponding river was included. Locations of river mouths are shown in Figure 1.

Rank	River	Δ CO ₂ Flux (Tg C yr ⁻¹)	Δ NPP (Tg C yr ⁻¹)
1	Amazon	+14.3	+113.6
2	Nile	+0.3	-0.1
3	Congo	+1.3	+12.4
4	Mississippi	-1.3	+26.4
5	Ob	+2	+2.2
6	Paraná	+0.5	+13.5
7	Yenisei	+2.6	+1.5
8	Lena	+2.8	+1.1
9	Niger	-0.1	+3
10	Yangtze	-3	+57.3
11	Amur	+0.7	+1.7
12	Mackenzie	+1.7	+0.6
13	Ganges	-11.7	+64.5
14	Zambezi	+0.1	+1
15	Indus	-0.7	+3.7
N/A	Total	+9.5	+302.4

3.3 Mechanisms of River-driven Air-sea CO₂ Flux

From January 2000 to December 2019, the time-mean surface-ocean DIC mass in DC_{run} increased by 370.7 Tg C. This triggered a solubility-pump-driven outgassing of 222.4 Tg C yr⁻¹ (Figure 4a). Over the same period, the addition of terrestrial nitrogen and silica, the sum of DN_{run} and DSi_{run}, drove a reduction of 21.5 Tg C in the surface-ocean DIC mass. Assuming the same ratio of surface-ocean DIC and air-sea CO₂ flux as in DC_{run}, the input of terrestrial nitrogen and silica will cause a CO₂ uptake of 12.9 Tg C yr⁻¹ (Figure 4b). Since the net ocean CO₂ uptake increased by 186.2 Tg C yr⁻¹ in response to terrestrial nitrogen and silica fertilization of NPP, the net increase in global CO₂ uptake is 173.3 Tg C yr⁻¹ (Figure 4c).

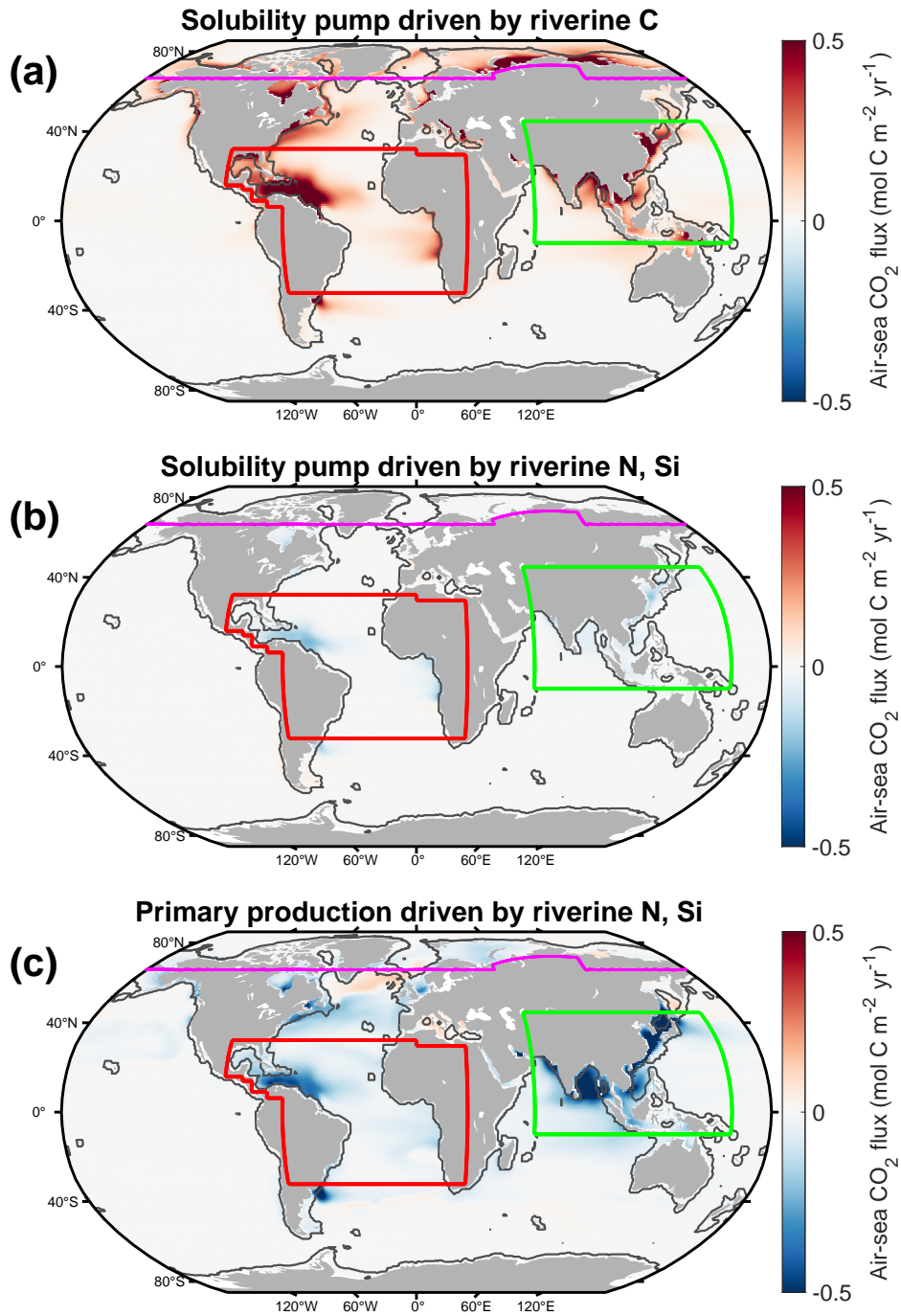


Figure 5. Climatological (January 2000 to December 2019) air-sea CO₂ flux associated with (a) change in the solubility pump driven by riverine carbon, (b) change in the solubility pump driven by riverine nitrogen and silica, and (c) NPP driven by riverine nitrogen and silica. Colored lines on maps show domains used for regional analysis. The black line delineates the coastal ocean from the open ocean.

365 Overall, the change in air-sea CO₂ flux driven by riverine exports was dominated
 366 1) by the solubility pump near river mouths in response to terrestrial carbon and 2) by
 367 NPP in the open ocean where CO₂ uptake from nitrogen- and silica-driven phytoplankton
 368 blooms exceeded riverine carbon-driven outgassing (Figure 4 and Figure 6). TROP-
 369 ATL and ARCT were dominated by riverine-driven CO₂ outgassing (71.9 and 24 Tg C
 370 yr⁻¹, respectively) and CO₂ uptake due to NPP fertilization in TROP-ATL and ARCT
 371 was minor (44.4 and 3.3 Tg C yr⁻¹, respectively). In SE-ASIA, the increase of CO₂ up-
 372 take due to enhanced NPP (69.6 Tg C yr⁻¹) exceeded CO₂ outgassing driven by river-
 373 ine carbon (53.9 Tg C yr⁻¹).

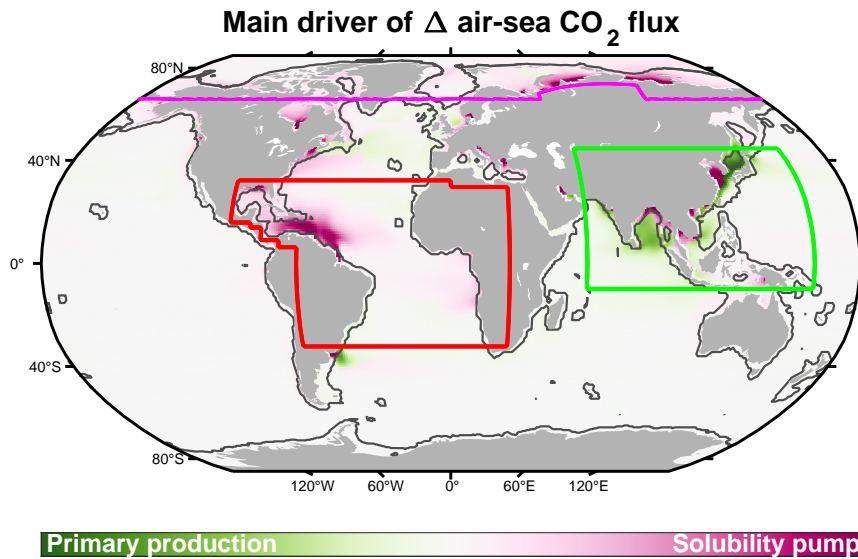


Figure 6. Pathways of change in climatological (January 2000 to December 2019) air-sea CO₂ flux driven by riverine exports. Colors represent the dominant flux shown in Figure 4. The black line delineates the coastal ocean from the open ocean.

374 4 Discussion

375 4.1 Fate of Riverine Dissolved Carbon and Nutrients

376 Once in the ocean, terrestrial dissolved carbon (t_{DOC} and t_{DIC}) result in a source
 377 of CO₂ to the atmosphere through a reduction of the solubility pump (Figure 7). Ter-
 378 restrial nutrients, such as nitrogen and silica (t_{DIN} , and t_{DSi}), fertilize phytoplankton
 379 and elevate CO₂ uptake via increased NPP.

380 The resultant export of marine organic carbon (m_{OC}) from the surface ocean drives
 381 additional CO₂ uptake via the solubility pump; at depth, the exported m_{OC} is reminer-
 382 alized to inorganic carbon (m_{IC}) (Figures 4b and 7). Thus, terrestrial nutrients have the

383 potential to shift riverine carbon-driven CO₂ outgassing to uptake, due to assimilation
 384 of carbon by primary producers. Despite a stronger increase of NPP in the coastal ocean
 385 (+5.2 g C m⁻² yr⁻¹, +7%) compared to the open ocean (+1 g C m⁻² yr⁻¹, +1%), the
 386 outgassing of CO₂ driven by riverine carbon through the solubility pump dominates changes
 387 in air-sea CO₂ flux close to river mouths. In contrast, the riverine nitrogen and silica sig-
 388 nal spreads further offshore and enhances NPP and CO₂ uptake — this mechanism domi-
 389 nates the change in air-sea CO₂ flux in open-ocean regions.

390 In carbon-dominated terrestrial margins, such as TROP-ATL and ARCT, rivers drive
 391 a large source of CO₂ from the ocean to the atmosphere. However, in nitrogen-dominated
 392 margins, such as SE-ASIA, the addition of lateral fluxes drives a substantial ocean car-
 393 bon sink. Globally, these two processes tend to compensate each other and our simula-
 394 tions suggest that the addition of riverine dissolved carbon, nitrogen, and silica result
 395 in a small net source of atmospheric CO₂ in the global ocean.

Table 4. Riverine exports loads.

Domain	Export (Tg yr ⁻¹)	ALL _{run}	Literature Value
Global	<i>t</i> _{DOC}	170.1	130–262 ¹
	<i>t</i> _{DIC}	381.8	320–453 ¹
	<i>t</i> _{DON}	11.7	11.8 ¹
	<i>t</i> _{DIN}	23.3	17–22.8 ¹
	<i>t</i> _{DSi}	139.7	158–171 ¹
ARCT	<i>t</i> _{DOC}	22.6	34–37.7 ²
	<i>t</i> _{DIC}	56.8	57 ²
	<i>t</i> _{DON}	1.4	0.05–0.84 ²
	<i>t</i> _{DIN}	1.1	0.04–0.43 ²
	<i>t</i> _{DSi}	12.6	11.4 ²
TROP-ATL	<i>t</i> _{DOC}	67.2	46 ³
	<i>t</i> _{DIC}	78.1	50 ³
	<i>t</i> _{DON}	4.2	N/A
	<i>t</i> _{DIN}	4.5	15.3 ³
	<i>t</i> _{DSi}	44.9	53 ³
SE-ASIA	<i>t</i> _{DOC}	36.6	N/A
	<i>t</i> _{DIC}	163.8	40 ⁴
	<i>t</i> _{DON}	2.6	N/A
	<i>t</i> _{DIN}	10.6	2.1–8.4 ^{4*}
	<i>t</i> _{DSi}	41.5	N/A

¹ (Drake et al., 2018; Mayorga et al., 2010; Frings et al., 2016; Sharples et al., 2017; Lacroix et al., 2020; Tivig et al., 2021; Tian et al., 2023; M. Li et al., 2017; Lacroix et al., 2020; Battin et al., 2023; Tian et al., 2023)

² (Manizza et al., 2011; Tank et al., 2012; Holmes et al., 2012; Le Fouest et al., 2013)

³ (Cotrim da Cunha et al., 2007; Araujo et al., 2014)

⁴ (Singh & Ramesh, 2011; H.-M. Li et al., 2014; J. Wang et al., 2020; Nishina et al., 2021; Piao et al., 2012; Patra et al., 2013)

* Computed from the sum of regional estimates

Table 5. Change in air-sea CO₂ flux and NPP driven by riverine exports.

Domain	$\Delta\text{CO}_2/\text{NPP}$	ALL_{run} (Pg C yr ⁻¹)	Literature Value (Pg C yr ⁻¹)
Global	ΔCO_2	+0.03	+0.11 ¹
	ΔNPP	+0.6	+0.6–3.9 ¹
ARCT	ΔCO_2	+22.8	+0.6–20 ^{2*}
	ΔNPP	+7.4	+58 ²
TROP-ATL	ΔCO_2	+20	+5–20 ^{3**}
	ΔNPP	+170	+80–400 ³
SE-ASIA	ΔCO_2	-24.7	N/A
	ΔNPP	+296	+100 ⁴

¹ (Tivig et al., 2021; Cotrim da Cunha et al., 2007)² (Manizza et al., 2011; Terhaar et al., 2021)³ (da Cunha & Buitenhuis, 2013; Louchard et al., 2021)⁴ (Tivig et al., 2021)* Effect of t_{DOC} only

** Lower bound is for smaller domain in western TROP-ATL

396 For both Baseline and ALL_{run} , the ocean CO₂ sink (2.55–2.58 Pg C yr⁻¹) lies within
397 the range of recent estimates (Resplandy et al., 2018; Regnier et al., 2022; Friedlingstein
398 et al., 2023). This present-day ocean CO₂ sink reflects the contribution of climate and
399 anthropogenic perturbations on top of preindustrial levels. In this study, a net riverine
400 carbon export of 0.55 Pg C yr⁻¹ (Table 1, $t_{DOC} + t_{DIC}$) drives a CO₂ outgassing of 0.22
401 Pg C yr⁻¹, while 35 Tg N yr⁻¹ (Table 1, $t_{DON} + t_{DIN}$) drives a CO₂ uptake of 0.17 Pg
402 C yr⁻¹ from enhanced ocean fertilization. We note that our multi-decadal estimates are
403 not in steady state and do have a realistic representation of estuarine, blue carbon, and
404 bottom sediment processes. Therefore, they are not directly comparable to steady-state,
405 pre-industrial estimates of the river loop (Resplandy et al., 2018).

406 The introduction of terrestrial nutrients, such as inorganic nitrogen and silica, in-
407 creased global-ocean marine NPP by 0.6 Pg C yr⁻¹ compared to Baseline. The addition
408 of t_{DIN} and t_{DON} also increased ocean NPP by 0.6 Pg C yr⁻¹ in the model described
409 in Tivig et al. (2021) (Table 5). The modeling study by Lacroix et al. (2020) also depicted
410 a 3% increase of ocean NPP in response to the addition of riverine nutrients. In our study,
411 the increase of NPP driven by riverine exports was stronger in the coastal ocean com-
412 pared to the open ocean, relative to their respective surface areas. This is consistent with
413 the recent study of Mathis et al. (2024), which demonstrates the role of increased river-
414 ine nutrient loads in driving stronger biological carbon fixation and thus an enhanced
415 CO₂ sink in the coastal ocean during the last century.

4.2 Spatial Variability

416
417 In this section, we analyze the impact of riverine exports on the spatial variability
418 of the ocean carbon cycle for our three regions of interest: ARCT, TROP-ATL, and SE-
419 ASIA.

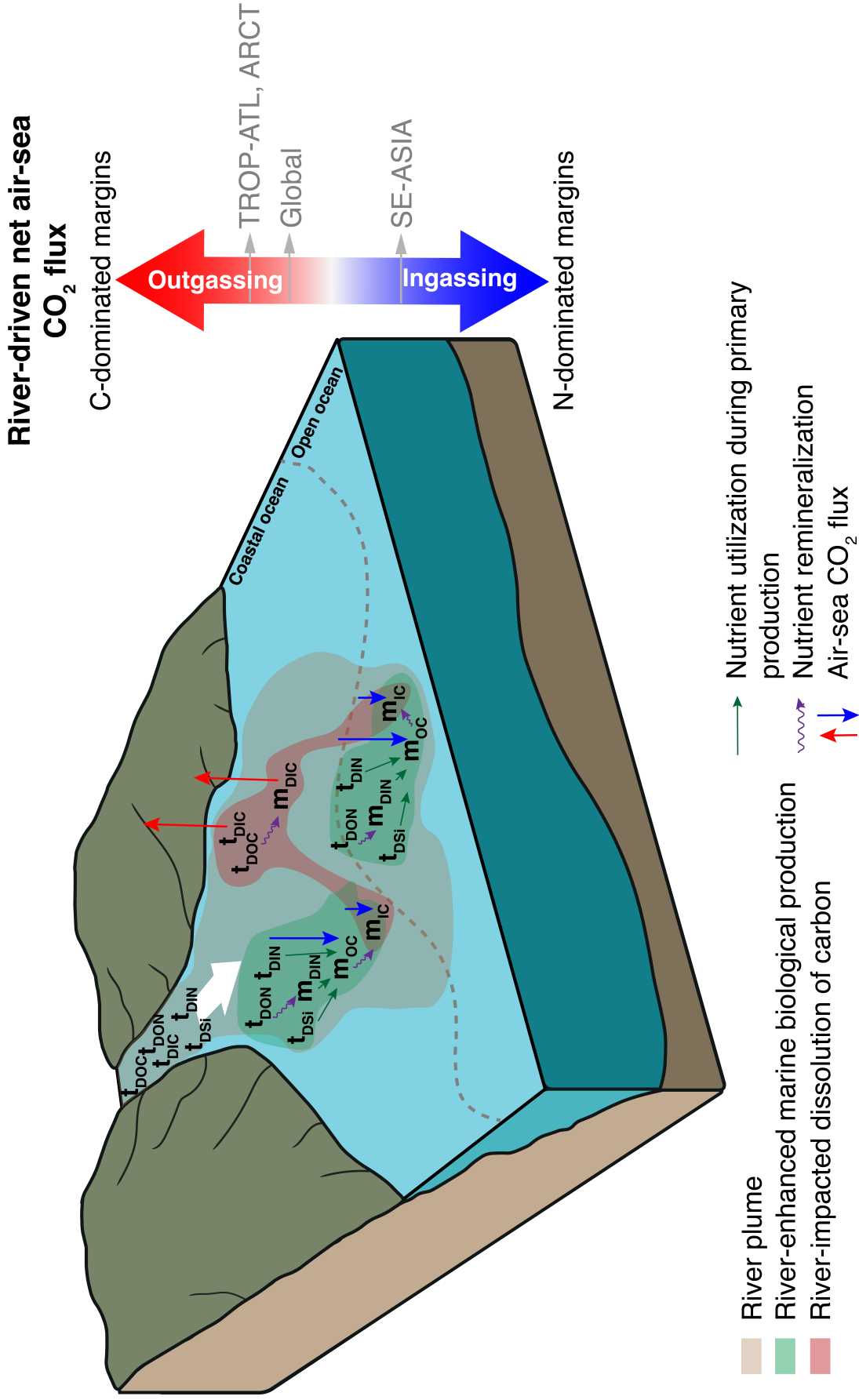


Figure 7. Fate of riverine exports in the coastal and open ocean. t_{DOC} : terrestrial DOC, t_{DIN} : terrestrial DIN, t_{DSi} : terrestrial DSi, t_{DIC} : terrestrial DIC, t_{DON} : terrestrial DON, m_{IC} : marine inorganic carbon, and m_{OC} : marine organic carbon. The dashed grey line delineates the coastal ocean from the open ocean.

4.2.1 Arctic Ocean (ARCT)

In the present study, the amount of freshwater, t_{DIC} , t_{DOC} , t_{DON} , t_{DIN} , and t_{DSi} delivered to the ARCT by individual rivers (Yenisey, Lena, Ob, and Mackenzie) falls within the range of observations from Tank et al. (2012), Le Fouest et al. (2013), and Holmes et al. (2012) (Supporting Information Table S1); suggesting that our estimates are reliable at the pan-Arctic scale (Table 4). In Baseline, ARCT uptakes $213.9 \text{ Tg C yr}^{-1}$ of atmospheric CO_2 . The addition of riverine exports reduces this CO_2 sink by 20 Tg C yr^{-1} and results in ECCO-Darwin having a more-consistent Arctic Ocean sink compared to previous studies (Manizza et al., 2011; Mortenson et al., 2020). In this region, riverine carbon dominates the response of air-sea CO_2 flux, with riverine t_{DOC} being responsible of 80% of CO_2 outgassing in ARCT. In Bertin et al. (2023), riverine exports from the Mackenzie River drove a CO_2 outgassing of roughly 0.5 Tg C yr^{-1} in the river plume. Our model depicts a CO_2 outgassing of similar magnitude in the river plume region ($\sim 0.1 \text{ Tg C yr}^{-1}$).

Due to anthropogenic climate change, thawing of carbon-rich permafrost is supplementing the load of t_{DOC} into Arctic rivers (Spencer et al., 2015). Permafrost-derived DOC has a relatively fast remineralization rate (~ 2 weeks) that could lead to strong CO_2 outgassing along coastal Arctic margins, which are dominated by permafrost-covered watersheds (Bertin et al., 2023). Furthermore, the degradation of organic carbon by microbial activity may be enhanced by changes in environmental conditions, such as increasing sea-surface temperature in ARCT (Carvalho & Wang, 2020). This would likely increase ocean CO_2 outgassing in response to the riverine carbon depicted in our study. Additionally, riverine nutrients also contribute to the Arctic Ocean carbon sink as they fertilize coastal waters. NPP in the Arctic Ocean increased by 3% ($+7.4 \text{ Tg C yr}^{-1}$) in ALL_{run} compared to Baseline. However, recent estimates by Terhaar et al. (2021) suggests that riverine nutrients support up to 9–11% ($+58 \text{ Tg C yr}^{-1}$) of marine NPP in the ARCT, in agreement with estimates by (Le Fouest et al., 2013, 2015) (Table 5). Therefore, CO_2 uptake driven by ocean fertilization from riverine nitrogen, and its capacity to compensate CO_2 outgassing in ARCT, might be underestimated in our study.

4.2.2 Tropical Atlantic (TROP-ATL)

Four of the top-15 global largest rivers (Amazon, Congo, Mississippi, and Niger) discharge into TROP-ATL. In total, rivers carry $67.2 \text{ Tg C yr}^{-1}$ as t_{DOC} , $78.1 \text{ Tg C yr}^{-1}$ as t_{DIC} , 4.2 Tg N yr^{-1} as t_{DON} , 4.5 Tg N yr^{-1} as t_{DIN} , and $44.9 \text{ Tg Si yr}^{-1}$ as t_{DSi} into TROP-ATL. Riverine t_{DOC} , t_{DIC} , and silica loads in our study are consistent with estimates from Cotrim da Cunha et al. (2007) and Araujo et al. (2014) (46 and $\sim 50 \text{ Tg C yr}^{-1}$ and 53 Tg Si yr^{-1} , respectively; Table 4). Our estimate of t_{DIN} delivered to this region is 3-fold lower than the value of $15.3 \text{ Tg N yr}^{-1}$ reported by Cotrim da Cunha et al. (2007) (Table 4). However, t_{DIN} export from the Amazon river (1 Tg N yr^{-1}) agrees well with Louchard et al. (2021) (0.9 Tg N yr^{-1}). A dynamic land ecosystem model that explicitly resolves fluxes over the entire watershed estimated that 0.9 Tg N yr^{-1} is exported as t_{DIN} from the Mississippi River (Tian et al., 2020), which is in general agreement with the 0.7 Tg N yr^{-1} that we use as input for our model. The load of t_{DIN} from the Congo River (0.2 Tg N yr^{-1}) is also the same order of magnitude compared to data from Jouanno et al. (2021). However, our Global-NEWS-2-based estimate of 0.1 Tg N yr^{-1} remains lower than previous estimates for the Niger River (Robertson & Rosswall, 1986) (0.5 Tg N yr^{-1}). We stress that in Africa river systems, nutrient loads are poorly constrained due to sparse data.

In Baseline, TROP-ATL is a source of CO_2 to the atmosphere ($0.10 \text{ Pg C yr}^{-1}$), which agrees with both interpolation-based products (Landschützer et al., 2016; Jersild et al., 2023; Rödenbeck, 2005) (0.04 – $0.08 \text{ Pg C yr}^{-1}$) and model results (da Cunha & Buitenhuis, 2013; Louchard et al., 2021) (0.03 – $0.04 \text{ Pg C yr}^{-1}$). We note that previous

471 studies show a river-driven increase in CO_2 uptake of 0.005 and 0.02 Pg C yr^{-1} when
 472 adding biogeochemical runoff in TROP-ATL and western TROP-ATL, respectively (da
 473 Cunha & Buitenhuis, 2013; Louchard et al., 2021). However, in our simulations, the ad-
 474 dition of riverine exports in ALL_{run} enhanced the source of CO_2 ($+0.02 \text{Pg C yr}^{-1}$) (Ta-
 475 ble 5).

476 Contrary to the estimates of Louchard et al. (2021), which include physical effects
 477 associated with freshwater, such as enhanced upper-ocean stratification and gas solubil-
 478 ity, our baseline simulation already includes these processes. Therefore, our suite of ex-
 479 periments cannot isolate and quantify the impact of freshwater discharge on ocean bio-
 480 geochemistry. Freshwater in river plumes facilitates the uptake of atmospheric CO_2 through
 481 the solubility pump, which in turn overlaps with the sink of CO_2 associated with bio-
 482 geochemical runoff. In addition to nitrogen, Louchard et al. (2021) also included inor-
 483 ganic phosphorus loads and a regionally-adjusted plankton ecosystem, e.g., by includ-
 484 ing a nitrogen-fixing phytoplankton functional type, which increased the model’s capa-
 485 bility to better resolve the biological pump and hence CO_2 uptake. For our simulations,
 486 we find that the increase of NPP associated with rivers in TROP-ATL (0.17Pg C yr^{-1})
 487 lies within the value of 0.08Pg C yr^{-1} reported in Louchard et al. (2021) (Table 5) and
 488 the value of 0.4Pg C yr^{-1} reported in Cotrim da Cunha et al. (2007). We note that hor-
 489 izontal resolution is also important for realistic representation of coastal processes. In
 490 their higher-resolution study, Louchard et al. (2021) were able to separately resolve the
 491 estuarine and plume/shelf waters of the Amazon River as a CO_2 source and sink, respec-
 492 tively, whereas our model intrinsically lacks such fine delineation.

493 The Amazon River clearly dominates the CO_2 outgassing signal in TROP-ATL, which
 494 is driven by the large load of t_{DOC} . Along with other rivers such as the Congo, Niger,
 495 and Orinoco Rivers, the Amazon River delivers a large amount of t_{DOC} , which originates
 496 from tropical forests. These forests contribute roughly one third of terrestrial NPP and
 497 their soil contains large amount of organic carbon, globally (Cleveland et al., 2010). As
 498 these watersheds are being drained by runoff from high precipitation, the subsequent high
 499 discharge, combined with carbon-rich soil and vegetation, leads to routing of t_{DOC} -rich
 500 waters to the coastal ocean (M. Li et al., 2019). At present time, it is critical to better
 501 constrain export of carbon from watersheds to coastal waters and characterize their fate
 502 in the ocean, as current efforts may be overestimating the land sink of carbon associated
 503 with tropical forests (Lauerwald et al., 2020). Additionally, the composition (refractory
 504 black carbon from combustion) and the quantity (CO_2 fertilization from NPP and soil
 505 erosion with deforestation) of carbon exports from the Amazon River remains uncertain
 506 due to ongoing changes in regional climate and fire regimes (Fleischer et al., 2019; Jones
 507 et al., 2020; Riquetti et al., 2023).

508 **4.2.3 Southeast Asia (SE-ASIA)**

509 Riverine biogeochemical runoff in SE-ASIA is dominated by high loads of t_{DIN} (10.6
 510 Tg N yr^{-1}) and t_{DIC} ($163.8 \text{Tg C yr}^{-1}$), especially from the Ganges and Yangtze Rivers.
 511 The magnitude of the riverine t_{DIN} load for SE-ASIA compares with individual estimates
 512 for the Bay of Bengal (0.4Tg N yr^{-1}), the Arabian Sea (0.06Tg N yr^{-1}), and the East
 513 China Sea ($1.6\text{--}7.9 \text{Tg N yr}^{-1}$) (Singh & Ramesh, 2011; H.-M. Li et al., 2014; J. Wang
 514 et al., 2020; Nishina et al., 2021) (Table 4). Our estimate of the t_{DIC} load in SE-ASIA
 515 remains higher than values reported in the literature ($\sim 40 \text{Tg C yr}^{-1}$) (Piao et al., 2012;
 516 Patra et al., 2013) and thus would require a regional adjustment as we did for the Ama-
 517 zon River (Table 4 and Supporting Information Text S1). This is explained by overes-
 518 timated t_{DIC} loads from the Yangtze (45.9Tg yr^{-1}) and the Ganges (18Tg yr^{-1}) Rivers
 519 compared to reported values (20 and $3\text{--}4 \text{Tg C yr}^{-1}$, respectively) (F. Wang et al., 2007;
 520 Guo et al., 2015; Y. Gao et al., 2017; Samanta et al., 2015). This overestimation is re-
 521 lated to the relationship based on river discharge and the dominant lithology (Amiotte Suchet
 522 et al., 2003; M. Li et al., 2017). Both rivers exhibit high discharge combined with weathering-

prone lithologies (carbonate rocks and shales for the Yangtze and Ganges rivers, respectively), which consume atmospheric CO₂ due to high rates of rock weathering (Amiotte Suchet et al., 2003). The Yangtze River is also known for its high river CO₂ emission flux due to the large permafrost area in the Qinghai-Tibet Plateau that releases large DIC loads during warm and rainy summer conditions (Song et al., 2020). As for ARCT, the t_{DIC} load from the Yangtze watershed remains uncertain, as its permafrost region is degrading quickly under the effect of climate warming (Cheng & Wu, 2007; Yang et al., 2010).

Similar to ARCT, SE-ASIA is a sink of atmospheric CO₂ in Baseline (0.3 Pg C yr⁻¹). Combining air-sea CO₂ budgets for the different regions composing SE-ASIA from literature (East-Pacific, Indonesian seas, and North Indian Ocean without including Oman and Somalian upwelling regions), we estimate a carbon sink of ~0.2 Pg C yr⁻¹ for the entire SE-ASIA domain (Kartadikaria et al., 2015; De Verneil et al., 2021; Zhong et al., 2022; Hood et al., 2023). Our study provides the first estimate of the contribution of present-day riverine exports to the carbon sink in SE-ASIA. The net air-sea CO₂ exchange balance driven by riverine exports in SE-ASIA results in a carbon sink of 0.02 Pg C yr⁻¹ in ALL_{run} . Compared to ARCT and TROP-ATL, carbon uptake in SE-ASIA is enhanced by a strong increase in marine NPP (+0.30 Pg C yr⁻¹, +9%) driven by riverine t_{DIN} . In Tivig et al. (2021), the simulated increase of NPP in response to riverine nitrogen was roughly 0.1 Pg C yr⁻¹ in Asia, with the strongest increase in the Yellow Sea, similar to our results (Table 5). Riverine nitrogen loads in this domain, and especially in the China seas, have been supplemented by increased nitrogen deposition, nitrogen fertilizer, manure, and human sewage over the last 50 years (Nishina et al., 2021). Even if nitrogen runoff is declining, agricultural-driven nitrogen loads will remain at significant levels and continue to fertilize phytoplankton blooms in this nitrogen-depleted marine region due to high denitrification (Michael Beman et al., 2005; Nishina et al., 2021). Locally, the addition of riverine biogeochemical runoff also drives a source of CO₂ to the atmosphere, which is primarily limited to near river mouth locations in SE-ASIA. In the Yellow Sea and the Northern Bay of Bengal, close to the Yangtze and Ganges Rivers, the addition of riverine exports at preindustrial levels in an ocean model also drove a CO₂ outgassing in Lacroix et al. (2020). Noticeably, in our simulations, riverine carbon turns the northern Bay of Bengal into a carbon source as suggested by Hood et al. (2023).

4.3 Model Improvements

Our study is a first attempt to add global, time-varying biogeochemical discharge in the ECCO-Darwin ocean carbon estimation framework. Here, we elaborate on some necessary, and potentially consequential, simplifications made in this study. In light of these simplifications, some next-step model improvements are described in Supporting Information Text S2.

Rivers are a significant source of phosphorus and iron that is pivotal for ocean biogeochemistry (Krachler et al., 2005; Tagliabue et al., 2017; Duhamel et al., 2021; Savenko & Savenko, 2021). Consequently, our results may underestimate the global-ocean air-sea CO₂ uptake due to the absence of riverine phosphorus or iron in the model, as they might be limiting for ocean NPP relative to the excess of terrestrial inorganic nitrogen. Additionally, riverine t_{ALK} flux was computed based on a constant ALK:DIC ratio, globally (0.98). We note that the GLORICH database used to compute the mean ALK:DIC ratio has relatively good coverage over the American continent but Eurasia and Africa are underrepresented (Hartmann et al., 2014). As such, the ALK:DIC ratio can vary substantially over regional scales. The lack of this spatially-granular information in our simulated exports may misrepresent riverine t_{ALK} fluxes and the alkalinity-driven buffering capacity of simulated river plumes (Dubois et al., 2010; Tank et al., 2012; Mol et al., 2018; Ghosh et al., 2021; Gomez et al., 2023). While in estuaries the absence of ALK relative to DIC leads to higher partial pressure of CO₂ (pCO₂) in upper-ocean waters and enhanced CO₂ outgassing, rivers also bring an excess of ALK relative to DIC on con-

575 tinentals shelves, which can reduce ocean $p\text{CO}_2$ through buffering and thus facilitate CO_2
 576 uptake (W.-J. Cai et al., 2010; Louchard et al., 2021). Furthermore, the fate of riverine
 577 t_{ALK} in the ocean is associated with the biological activity of calcifying organisms and
 578 exchange at the sediment-water interface (Middelburg et al., 2020) — an undergoing de-
 579 velopment in our modeling system.

580 In our model, the global-ocean net CO_2 outgassing driven by riverine exports re-
 581 flects the stronger effect of riverine carbon on the solubility pump (CO_2 source) com-
 582 pared to the change in the CO_2 uptake associated with the increase in NPP. This im-
 583 balance can result from an overestimation of CO_2 outgassing driven by riverine carbon,
 584 and especially t_{DOC} . First, assuming that total loads of carbon or nutrients over each
 585 watershed are routed to the ocean is a misrepresentation, as losses and gains occur through
 586 the LOAC (W.-J. Cai, 2011). Second, t_{DOC} is degraded in coastal waters at different
 587 rates depending on its origin and subsequent labile fraction (Lønborg et al., 2020). In
 588 the present study, in addition to not accounting for refractory and labile fractions of t_{DOC} ,
 589 marine and terrestrial DOC are both being remineralized at the same rate (3 months).
 590 Overall, this could lead to an overestimation of t_{DOC} remineralization and thus ocean
 591 CO_2 outgassing due to the subsequent excess of DIC. For instance, the Amazon River
 592 — the main source of riverine t_{DOC} into the ocean — contributes to almost 50% (+0.014
 593 Pg C yr^{-1}) of the global-ocean CO_2 outgassing in response to riverine exports in our study.
 594 However, t_{DOC} from the Amazon River shows stronger stability in the coastal ocean and
 595 is exported from the continental margin to the open ocean (Medeiros et al., 2015; Louchard
 596 et al., 2021). Increasing the refractory pool of Amazon t_{DOC} could therefore decrease
 597 CO_2 outgassing in our simulations. While recent modeling studies include separate pools
 598 of refractory and labile t_{DOC} with different remineralization rates at regional scales (Louchard
 599 et al., 2021; Gibson et al., 2022; Bertin et al., 2023), the nature of t_{DOC} needs to be bet-
 600 ter accounted for in global-ocean biogeochemistry models.

601 5 Perspectives

602 Biogeochemical inputs from rivers into the ocean are subject to variability from cli-
 603 mate change and/or human activities. Over the last century, loads of riverine exports
 604 such as nitrogen and phosphorus increased dramatically — mostly due to anthropogenic
 605 perturbations (+349% and +233%, respectively) (Lacroix et al., 2021). In the coastal
 606 ocean, this has strongly increased NPP associated with the regions in which our model
 607 depicts the strongest impact of riverine nutrients on NPP (TROP-ATL and SE-ASIA)
 608 (Lacroix et al., 2021). Over the past 20 years, fertilizers and aquaculture have been iden-
 609 tified as global drivers of phytoplankton blooms in coastal waters (Dai et al., 2023). The
 610 load of riverine t_{DOC} also increased globally over the period 1860–2010 (+17%), due to
 611 CO_2 fertilization of terrestrial vegetation and climate change (Nakhavali et al., 2024).
 612 In the near future (2050), the global contribution of natural sources of nitrogen and phos-
 613 phorus in riverine inputs is expected to continue to decrease due to land-use change, while
 614 anthropogenic sources from human waste, agriculture, and aquaculture are projected to
 615 increase for every potential Shared Socioeconomic Pathways (SSP) scenario (Beusen et
 616 al., 2022). However, the export of nutrients from anthropogenic sources to the ocean will
 617 decrease in industrialized regions such as North America, Europe (including the Russian
 618 Federation), Japan, and Oceania in most SSPs (Beusen & Bouwman, 2022). For instance,
 619 in the contiguous United States, the riverine load of nitrogen from human waste and at-
 620 mospheric pollution decreased over 1930–2017 (Byrnes et al., 2020). Nonetheless, the load
 621 of nitrogen from agricultural sources kept increasing over the same period (Byrnes et al.,
 622 2020). Consequently, only the long-term adoption of the Paris Agreement and sustain-
 623 able development scenarios, such as SSP1 where the use of resources and the dependency
 624 on fossil fuels are significantly reduced, would lead to better stream water quality (Beusen
 625 & Bouwman, 2022; Beusen et al., 2022). Over the 21st century, the increase of ocean NPP
 626 and the associated carbon sink driven by the historical increase of nutrients loads is ex-

pected to be dampened by the increase of CO₂ outgassing from elevated terrestrial organic matter loads (S. Gao et al., 2023).

Depicting the role of riverine exports in the ocean carbon cycle remains limited by the spatial and temporal coverage/resolution of models, forcing products, and observations. As river discharge is associated with suspended particulate loads, ocean color retrievals from spaceborne instruments can be an effective tool for monitoring river plumes systems. However, the complexity of optical properties and their large space-time variability requires high-resolution sensors to capture the actual constituents of ocean biogeochemistry. The recently launched Plankton, Aerosol, Cloud, ocean Ecosystem (PACE) satellite mission (<https://pace.oceansciences.org/>) and its onboard high-resolution spectrometer will bring new insights into the water quality of coastal regions near river mouths. Combined, with river discharge retrievals from the Surface Water and Ocean Topography (SWOT, <https://swot.jpl.nasa.gov/>), combined spaceborne observations of ocean color and terrestrial fluxes of freshwater into the ocean will pave the way for an integrated Earth Observation System, where the connection between the land and the ocean will be better understood. While effective, these satellite missions are expensive and should not replace critical in-situ and ground-truthed observations. We highlight that ambitious spaceborne missions can indeed be complemented by more modest initiatives, such as citizen science or stakeholder engagement to monitor water quality in river systems (Abbott et al., 2018).

6 Conclusion

Our simulations suggest that the role of present-day riverine exports is moderate, with an outgassing of 0.03 Pg C yr⁻¹ to the atmosphere, globally. We find that riverine inputs drive contrasting regional patterns in air-sea CO₂ flux. Terrestrial dissolved carbon, and especially t_{DOC}, contributes to an outgassing of CO₂ through a reduction of the ocean's solubility pump. Terrestrial nutrients, and in particular t_{DIN}, fertilizes phytoplankton and increases marine NPP and the associated carbon biomass. Thus, terrestrial nutrients such as inorganic nitrogen and silica enhance the uptake of atmospheric CO₂ into the ocean. While outgassing of CO₂ is primarily located near river mouths, the fertilization by riverine nitrogen and silica spreads further offshore and into the open ocean. In carbon-dominated margins such as ARCT or TROP-ATL, rivers contribute a large source of CO₂ from the ocean to the atmosphere. However, in nitrogen-dominated margins such as SE-ASIA, rivers drive a large sink of atmospheric CO₂ into the ocean. This work highlights that a better quantification of lateral riverine exports and the incorporation of these fluxes in global models is pivotal for regional and global carbon budgets. Conducting sensitivity experiments could support national policy decisions and inform climate resilience strategies for land and marine practices.

Acknowledgments

A portion of this research was carried out at the Jet Propulsion Laboratory, California Institute of Technology, under a contract with the National Aeronautics and Space Administration (80NM0018D0004). Support from the Carbon Cycle Science (CCS) and Carbon Monitoring Systems (CMS) programs are acknowledged. High-end computing resources were provided by the NASA Advanced Supercomputing (NAS) Division of the Ames Research Center. Government sponsorship acknowledged. © 2024. All rights reserved

Open Research

ECCO-Darwin model output is available at the ECCO Data Portal: <http://data.nas.nasa.gov/ecco/>. Model code and platform-independent instructions for running the ECCO-Darwin sim-

675 uations used in this paper and generating runoff forcing are available at: 10.5281/zen-
676 do.10562713.

677 References

- 678 Abbott, B. W., Moatar, F., Gauthier, O., Fovet, O., Antoine, V., & Ragueneau,
679 O. (2018). Trends and seasonality of river nutrients in agricultural catch-
680 ments: 18years of weekly citizen science in france. *Science of The Total En-*
681 *vironment*, *624*, 845-858. Retrieved from [https://www.sciencedirect.com/](https://www.sciencedirect.com/science/article/pii/S0048969717336033)
682 [science/article/pii/S0048969717336033](https://www.sciencedirect.com/science/article/pii/S0048969717336033) doi: [https://doi.org/10.1016/](https://doi.org/10.1016/j.scitotenv.2017.12.176)
683 [j.scitotenv.2017.12.176](https://doi.org/10.1016/j.scitotenv.2017.12.176)
- 684 Amiotte Suchet, P., Probst, J.-L., & Ludwig, W. (2003). Worldwide distribution
685 of continental rock lithology: Implications for the atmospheric/soil co2 uptake
686 by continental weathering and alkalinity river transport to the oceans. *Global*
687 *Biogeochemical Cycles*, *17*(2).
- 688 Andrews, A., Kofler, J., Trudeau, M., Williams, J., Neff, D., Masarie, K., ... oth-
689 ers (2014). Co 2, co, and ch 4 measurements from tall towers in the noaa earth
690 system research laboratory's global greenhouse gas reference network: Instru-
691 mentation, uncertainty analysis, and recommendations for future high-accuracy
692 greenhouse gas monitoring efforts. *Atmospheric Measurement Techniques*, *7*(2),
693 647–687.
- 694 Araujo, M., Noriega, C., & Lefèvre, N. (2014). Nutrients and carbon fluxes in the
695 estuaries of major rivers flowing into the tropical atlantic. *Frontiers in Marine*
696 *Science*, *1*. Retrieved from [https://www.frontiersin.org/articles/10.3389/](https://www.frontiersin.org/articles/10.3389/fmars.2014.00010)
697 [fmars.2014.00010](https://www.frontiersin.org/articles/10.3389/fmars.2014.00010) doi: [10.3389/fmars.2014.00010](https://doi.org/10.3389/fmars.2014.00010)
- 698 Battin, T. J., Lauerwald, R., Bernhardt, E. S., Bertuzzo, E., Gener, L. G., Hall Jr,
699 R. O., ... others (2023). River ecosystem metabolism and carbon biogeochemistry
700 in a changing world. *Nature*, *613*(7944), 449–459.
- 701 Bertin, C., Carroll, D., Menemenlis, D., Dutkiewicz, S., Zhang, H., Matsuoka, A., ...
702 others (2023). Biogeochemical river runoff drives intense coastal arctic ocean co2
703 outgassing. *Geophysical Research Letters*, *50*(8), e2022GL102377.
- 704 Beusen, A. H. W., & Bouwman, A. F. (2022). Future projections of river nutri-
705 ent export to the global coastal ocean show persisting nitrogen and phosphorus
706 distortion. *Frontiers in Water*, *4*, 893585.
- 707 Beusen, A. H. W., Doelman, J. C., Van Beek, L. P. H., Van Puijenbroek,
708 P. J. T. M., Mogollón, J. M., Van Grinsven, H. J. M., ... Bouwman, A. F. (2022).
709 Exploring river nitrogen and phosphorus loading and export to global coastal wa-
710 ters in the shared socio-economic pathways. *Global Environmental Change*, *72*,
711 102426.
- 712 Bloom, A. A., Bowman, K. W., Liu, J., Konings, A. G., Worden, J. R., Parazoo,
713 N. C., ... others (2020). Lagged effects regulate the inter-annual variability of the
714 tropical carbon balance. *Biogeosciences*, *17*(24), 6393–6422.
- 715 Brix, H., Menemenlis, D., Hill, C., Dutkiewicz, S., Jahn, O., Wang, D., ... Zhang,
716 H. (2015). Using green's functions to initialize and adjust a global, eddying ocean
717 biogeochemistry general circulation model. *Ocean Modelling*, *95*, 1–14.
- 718 Byrnes, D. K., Van Meter, K. J., & Basu, N. B. (2020). Long-term shifts in u.s. ni-
719 trogen sources and sinks revealed by the new trend-nitrogen data set (1930–2017).
720 *Global Biogeochemical Cycles*, *34*(9), e2020GB006626. Retrieved from
721 <https://agupubs.onlinelibrary.wiley.com/doi/abs/10.1029/2020GB006626>
722 <https://agupubs.onlinelibrary.wiley.com/doi/abs/10.1029/2020GB006626>
(e2020GB006626 2020GB006626) doi: <https://doi.org/10.1029/2020GB006626>
- 723 Cai, W., Chen, C. A., & Borges, A. (2013). Carbon dioxide dynamics and fluxes
724 in coastal waters influenced by river plumes. *Biogeochemical Dynamics at Major*
725 *River-Coastal Interfaces*, edited by: Bianchi, TS, Allison MA, and Cai, W.-J.,
726 Cambridge University Press, Cambridge, 155–173.

- 727 Cai, W.-J. (2011). Estuarine and coastal ocean carbon paradox: Co₂ sinks or sites of
728 terrestrial carbon incineration? *Annual review of marine science*, *3*, 123–145.
- 729 Cai, W.-J., Hu, X., Huang, W.-J., Jiang, L.-Q., Wang, Y., Peng, T.-H., & Zhang,
730 X. (2010). Alkalinity distribution in the western north atlantic ocean margins.
731 *Journal of Geophysical Research: Oceans*, *115*(C8). Retrieved from
732 <https://agupubs.onlinelibrary.wiley.com/doi/abs/10.1029/2009JC005482>
733 doi: <https://doi.org/10.1029/2009JC005482>
- 734 Calmels, D., Gaillardet, J., Brenot, A., & France-Lanord, C. (2007). Sustained sul-
735 fide oxidation by physical erosion processes in the mackenzie river basin: Climatic
736 perspectives. *Geology*, *35*(11), 1003–1006.
- 737 Carroll, D., Menemenlis, D., Adkins, J., Bowman, K., Brix, H., Dutkiewicz, S., ...
738 others (2020). The ecco-darwin data-assimilative global ocean biogeochemistry
739 model: Estimates of seasonal to multidecadal surface ocean pco₂ and air-sea co₂
740 flux. *Journal of Advances in Modeling Earth Systems*, *12*(10), e2019MS001888.
- 741 Carroll, D., Menemenlis, D., Dutkiewicz, S., Lauderdale, J. M., Adkins, J. F.,
742 Bowman, K. W., ... others (2022). Attribution of space-time variability in
743 global-ocean dissolved inorganic carbon. *Global biogeochemical cycles*, *36*(3),
744 e2021GB007162.
- 745 Carroll, D., Menemenlis, D., Zhang, H., Mazloff, M., McKinley, G., Fay, A., ...
746 Fenty, I. (2024, February). *Evaluation of the ECCO-Darwin Ocean Biogeo-*
747 *chemistry State Estimate vs. In-situ Observations*. Zenodo. Retrieved from
748 <https://doi.org/10.5281/zenodo.10627664> doi: 10.5281/zenodo.10627664
- 749 Carvalho, K., & Wang, S. (2020). Sea surface temperature variability in
750 the arctic ocean and its marginal seas in a changing climate: Patterns and
751 mechanisms. *Global and Planetary Change*, *193*, 103265. Retrieved from
752 <https://www.sciencedirect.com/science/article/pii/S0921818120301569>
753 doi: <https://doi.org/10.1016/j.gloplacha.2020.103265>
- 754 Cheng, G., & Wu, T. (2007). Responses of permafrost to climate change and their
755 environmental significance, qinghai-tibet plateau. *Journal of Geophysical Research:*
756 *Earth Surface*, *112*(F2).
- 757 Cleveland, C. C., Wieder, W. R., Reed, S. C., & Townsend, A. R. (2010). Experi-
758 mental drought in a tropical rain forest increases soil carbon dioxide losses to the
759 atmosphere. *Ecology*, *91*(8), 2313–2323.
- 760 Cotrim da Cunha, L., Buitenhuis, E. T., Le Quéré, C., Giraud, X., & Ludwig, W.
761 (2007). Potential impact of changes in river nutrient supply on global ocean
762 biogeochemistry. *Global Biogeochemical Cycles*, *21*(4).
- 763 da Cunha, L. C., & Buitenhuis, E. (2013). Riverine influence on the tropical atlantic
764 ocean biogeochemistry. *Biogeosciences*, *10*(10), 6357–6373.
- 765 Dai, Y., Yang, S., Zhao, D., Hu, C., Xu, W., Anderson, D. M., ... others (2023).
766 Coastal phytoplankton blooms expand and intensify in the 21st century. *Nature*,
767 *615*(7951), 280–284.
- 768 De Verneil, A., Lachkar, Z., Smith, S., & Lévy, M. (2021). Evaluating the arabian
769 sea as a regional source of atmospheric co₂: seasonal variability and drivers. *Bio-*
770 *geosciences Discussions*, *2021*, 1–38.
- 771 Drake, T. W., Raymond, P. A., & Spencer, R. G. (2018). Terrestrial carbon inputs
772 to inland waters: A current synthesis of estimates and uncertainty. *Limnology and*
773 *Oceanography Letters*, *3*(3), 132–142.
- 774 Dubois, K. D., Lee, D., & Veizer, J. (2010). Isotopic constraints on alkalinity, dis-
775 solved organic carbon, and atmospheric carbon dioxide fluxes in the mississippi
776 river. *Journal of Geophysical Research: Biogeosciences*, *115*(G2). Retrieved from
777 <https://agupubs.onlinelibrary.wiley.com/doi/abs/10.1029/2009JG001102>
778 doi: <https://doi.org/10.1029/2009JG001102>
- 779 Duhamel, S., Diaz, J. M., Adams, J. C., Djaoudi, K., Steck, V., & Waggoner, E. M.
780 (2021). Phosphorus as an integral component of global marine biogeochemistry.

- 781 *Nature Geoscience*, 14(6), 359–368.
- 782 Fekete, B. M., Vörösmarty, C. J., & Grabs, W. (2002). High-resolution fields of
783 global runoff combining observed river discharge and simulated water balances.
784 *Global Biogeochemical Cycles*, 16(3), 15–1–15–10.
- 785 Feng, Y., Menemenlis, D., Xue, H., Zhang, H., Carroll, D., Du, Y., & Wu, H. (2021).
786 Improved representation of river runoff in estimating the circulation and climate
787 of the ocean version 4 (eccov4) simulations: implementation, evaluation, and
788 impacts to coastal plume regions. *Geoscientific Model Development*, 14(3), 1801–
789 1819.
- 790 Fennel, K., & Testa, J. M. (2019). Biogeochemical controls on coastal hypoxia. *An-*
791 *ual review of marine science*, 11, 105–130.
- 792 Fleischer, K., Rammig, A., De Kauwe, M. G., Walker, A. P., Domingues, T. F.,
793 Fuchslueger, L., ... others (2019). Amazon forest response to co2 fertilization
794 dependent on plant phosphorus acquisition. *Nature Geoscience*, 12(9), 736–741.
- 795 Follows, M. J., Ito, T., & Dutkiewicz, S. (2006). On the solution of the carbon-
796 ate chemistry system in ocean biogeochemistry models. *Ocean Modelling*, 12(3-4),
797 290–301.
- 798 Forget, G., Campin, J.-M., Heimbach, P., Hill, C., Ponte, R., & Wunsch, C. (2015).
799 Ecco version 4: An integrated framework for non-linear inverse modeling and
800 global ocean state estimation. *Geoscientific Model Development*, 8(10), 3071–
801 3104.
- 802 Friedlingstein, P., O’sullivan, M., Jones, M. W., Andrew, R. M., Bakker, D. C.,
803 Hauck, J., ... others (2023). Global carbon budget 2023. *Earth System Science*
804 *Data*, 15(12), 5301–5369.
- 805 Frings, P. J., Clymans, W., Fontorbe, G., Christina, L., & Conley, D. J. (2016). The
806 continental si cycle and its impact on the ocean si isotope budget. *Chemical Geol-*
807 *ogy*, 425, 12–36.
- 808 Gao, S., Schwinger, J., Tjiputra, J., Bethke, I., Hartmann, J., Mayorga, E., &
809 Heinze, C. (2023). Riverine impact on future projections of marine primary
810 production and carbon uptake. *Biogeosciences*, 20(1), 93–119.
- 811 Gao, Y., Yang, T., Wang, Y., & Yu, G. (2017). Fate of river-transported carbon
812 in china: implications for carbon cycling in coastal ecosystems. *Ecosystem Health*
813 *and Sustainability*, 3(3), e01265. Retrieved from [https://spj.science.org/doi/](https://spj.science.org/doi/abs/10.1002/ehs2.1265)
814 [abs/10.1002/ehs2.1265](https://spj.science.org/doi/abs/10.1002/ehs2.1265) doi: 10.1002/ehs2.1265
- 815 Gaspar, P., Grégoris, Y., & Lefevre, J.-M. (1990). A simple eddy kinetic energy
816 model for simulations of the oceanic vertical mixing: Tests at station papa and
817 long-term upper ocean study site. *Journal of Geophysical Research: Oceans*,
818 95(C9), 16179–16193.
- 819 Ghosh, J., Chakraborty, K., Chanda, A., Akhand, A., Bhattacharya, T., Das, S.,
820 ... Wells, M. (2021). Outwelling of total alkalinity and dissolved inorganic car-
821 bon from the hooghly river to the adjacent coastal bay of bengal. *Environmental*
822 *Monitoring and Assessment*, 193(7), 415.
- 823 Gibson, G. A., Elliot, S., Clement Kinney, J., Piliouras, A., & Jeffery, N. (2022). As-
824 sessing the potential impact of river chemistry on arctic coastal production. *Fron-*
825 *tiers in Marine Science*, 9, 738363. Retrieved from [https://www.frontiersin](https://www.frontiersin.org/articles/10.3389/fmars.2022.738363)
826 [.org/articles/10.3389/fmars.2022.738363](https://www.frontiersin.org/articles/10.3389/fmars.2022.738363) doi: 10.3389/fmars.2022.738363
- 827 Gomez, F. A., Lee, S.-K., Stock, C. A., Ross, A. C., Resplandy, L., Siedlecki, S. A.,
828 ... Salisbury, J. E. (2023). Rc4uscoast: a river chemistry dataset for regional
829 ocean model applications in the us east coast, gulf of mexico, and us west coast.
830 *Earth System Science Data*, 15(5), 2223–2234.
- 831 Guo, J., Wang, F., Vogt, R. D., Zhang, Y., & Liu, C.-Q. (2015). Anthropogenically
832 enhanced chemical weathering and carbon evasion in the yangtze basin. *Scientific*
833 *reports*, 5(1), 11941.
- 834 Hagemann, S., & Dümenil, L. (1997). A parametrization of the lateral waterflow for

- 835 the global scale. *Climate dynamics*, *14*, 17–31.
- 836 Hagemann, S., & Gates, L. D. (2003). Improving a subgrid runoff parameterization
837 scheme for climate models by the use of high resolution data derived from satellite
838 observations. *Climate Dynamics*, *21*, 349–359.
- 839 Hartmann, J., Jansen, N., Dürr, H. H., Kempe, S., & Köhler, P. (2009). Global co2-
840 consumption by chemical weathering: What is the contribution of highly active
841 weathering regions? *Global and Planetary Change*, *69*(4), 185–194.
- 842 Hartmann, J., Lauerwald, R., & Moosdorf, N. (2014). A brief overview of the global
843 river chemistry database, glorch. *Procedia Earth and Planetary Science*, *10*, 23–
844 27.
- 845 Holmes, R. M., McClelland, J. W., Peterson, B. J., Tank, S. E., Bulygina, E., Eglinton,
846 T. I., ... others (2012). Seasonal and annual fluxes of nutrients and organic
847 matter from large rivers to the arctic ocean and surrounding seas. *Estuaries and
848 Coasts*, *35*, 369–382.
- 849 Hood, R. R., Rixen, T., Levy, M., Hansell, D. A., Coles, V. J., & Lachkar, Z. (2023).
850 *Oxygen, carbon and ph variability in the indian ocean*. Elsevier.
- 851 Ianson, D., Feely, R. A., Sabine, C. L., & Juranek, L. W. (2009). Features of coastal
852 upwelling regions that determine net air-sea co 2 flux. *Journal of oceanography*,
853 *65*, 677–687.
- 854 Jersild, A., Landschützer, P., Gruber, N., & Bakker, D. (2023). *An observation-based
855 global monthly gridded sea surface pco2 and air-sea co2 flux product from 1982
856 onward and its monthly climatology* (Vol. 160558).
- 857 Jones, M. W., Coppola, A. I., Santín, C., Dittmar, T., Jaffé, R., Doerr, S. H., &
858 Quine, T. A. (2020). Fires prime terrestrial organic carbon for riverine export to
859 the global oceans. *Nature communications*, *11*(1), 2791.
- 860 Jouanno, J., Moquet, J.-S., Berline, L., Radenac, M.-H., Santini, W., Changeux, T.,
861 ... others (2021). Evolution of the riverine nutrient export to the tropical atlantic
862 over the last 15 years: is there a link with sargassum proliferation? *Environmental
863 Research Letters*, *16*(3), 034042.
- 864 Kartadikaria, A. R., Watanabe, A., Nadaoka, K., Adi, N. S., Prayitno, H. B., Soe-
865 morumekso, S., ... others (2015). Co2 sink/source characteristics in the tropical
866 indonesian seas. *Journal of Geophysical Research: Oceans*, *120*(12), 7842–7856.
- 867 Krachler, R., Jirsa, F., & Ayromlou, S. (2005). Factors influencing the dissolved iron
868 input by river water to the open ocean. *Biogeosciences*, *2*(4), 311–315.
- 869 Krinner, G., Viovy, N., de Noblet-Ducoudré, N., Ogée, J., Polcher, J., Friedlingstein,
870 P., ... Prentice, I. C. (2005). A dynamic global vegetation model for studies of
871 the coupled atmosphere-biosphere system. *Global Biogeochemical Cycles*, *19*(1).
- 872 Lacroix, F., Ilyina, T., & Hartmann, J. (2020). Oceanic co 2 outgassing and bio-
873 logical production hotspots induced by pre-industrial river loads of nutrients and
874 carbon in a global modeling approach. *Biogeosciences*, *17*(1), 55–88.
- 875 Lacroix, F., Ilyina, T., Mathis, M., Laruelle, G. G., & Regnier, P. (2021). Histor-
876 ical increases in land-derived nutrient inputs may alleviate effects of a changing
877 physical climate on the oceanic carbon cycle. *Global change biology*, *27*(21),
878 5491–5513.
- 879 Landschützer, P., Gruber, N., & Bakker, D. C. (2016). Decadal variations and
880 trends of the global ocean carbon sink. *Global Biogeochemical Cycles*, *30*(10),
881 1396–1417.
- 882 Laruelle, G. G., Goossens, N., Arndt, S., Cai, W.-J., & Regnier, P. (2017). Air-
883 water co 2 evasion from us east coast estuaries. *Biogeosciences*, *14*(9), 2441–2468.
- 884 Lauerwald, R., Regnier, P., Guenet, B., Friedlingstein, P., & Ciais, P. (2020). How
885 simulations of the land carbon sink are biased by ignoring fluvial carbon transfers:
886 A case study for the amazon basin. *One Earth*, *3*(2), 226–236. Retrieved from
887 <https://www.sciencedirect.com/science/article/pii/S2590332220303535>
888 doi: <https://doi.org/10.1016/j.oneear.2020.07.009>

- 889 Laurent, A., Fennel, K., Cai, W.-J., Huang, W.-J., Barbero, L., & Wanninkhof,
890 R. (2017). Eutrophication-induced acidification of coastal waters in the north-
891 ern gulf of mexico: Insights into origin and processes from a coupled physical-
892 biogeochemical model. *Geophysical Research Letters*, *44*(2), 946–956.
- 893 Lee, R. Y., Seitzinger, S., & Mayorga, E. (2016). Land-based nutrient loading to
894 lmes: a global watershed perspective on magnitudes and sources. *Environmental*
895 *development*, *17*, 220–229.
- 896 Le Fouest, V., Babin, M., & Tremblay, J.-É. (2013). The fate of riverine nutrients on
897 arctic shelves. *Biogeosciences*, *10*(6), 3661–3677.
- 898 Le Fouest, V., Manizza, M., Tremblay, B., & Babin, M. (2015). Modelling
899 the impact of riverine don removal by marine bacterioplankton on primary
900 production in the arctic ocean. *Biogeosciences*, *12*(11), 3385–3402. Re-
901 trieved from <https://bg.copernicus.org/articles/12/3385/2015/> doi:
902 10.5194/bg-12-3385-2015
- 903 Li, H.-M., Tang, H.-J., Shi, X.-Y., Zhang, C.-S., & Wang, X.-L. (2014). Increased
904 nutrient loads from the changjiang (yangtze) river have led to increased harmful
905 algal blooms. *Harmful Algae*, *39*, 92–101.
- 906 Li, M., Peng, C., Wang, M., Xue, W., Zhang, K., Wang, K., ... Zhu, Q. (2017). The
907 carbon flux of global rivers: A re-evaluation of amount and spatial patterns. *Eco-*
908 *logical Indicators*, *80*, 40–51.
- 909 Li, M., Peng, C., Zhou, X., Yang, Y., Guo, Y., Shi, G., & Zhu, Q. (2019). Mod-
910 eling global riverine doc flux dynamics from 1951 to 2015. *Journal of Ad-*
911 *vances in Modeling Earth Systems*, *11*(2), 514-530. Retrieved from [https://](https://agupubs.onlinelibrary.wiley.com/doi/abs/10.1029/2018MS001363)
912 agupubs.onlinelibrary.wiley.com/doi/abs/10.1029/2018MS001363 doi:
913 <https://doi.org/10.1029/2018MS001363>
- 914 Lønborg, C., Carreira, C., Jickells, T., & Álvarez-Salgado, X. A. (2020, jun). Im-
915 pacts of Global Change on Ocean Dissolved Organic Carbon (DOC) Cycling.
916 *Frontiers in Marine Science*, *7*. doi: 10.3389/fmars.2020.00466
- 917 Louchard, D., Gruber, N., & Münnich, M. (2021). The impact of the amazon on
918 the biological pump and the air-sea co2 balance of the western tropical atlantic.
919 *Global Biogeochemical Cycles*, *35*(6), e2020GB006818.
- 920 Maavara, T., Lauerwald, R., Regnier, P., & Van Cappellen, P. (2017). Global pertur-
921 bation of organic carbon cycling by river damming. *Nature communications*, *8*(1),
922 15347.
- 923 Mahowald, N. M., Engelstaedter, S., Luo, C., Sealy, A., Artaxo, P., Benitez-Nelson,
924 C., ... others (2009). Atmospheric iron deposition: global distribution, variability,
925 and human perturbations. *Annual review of marine science*, *1*, 245–278.
- 926 Manizza, M., Follows, M. J., Dutkiewicz, S., Menemenlis, D., McClelland, J. W.,
927 Hill, C. N., ... Key, R. M. (2011). A model of the arctic ocean carbon cy-
928 cle. *Journal of Geophysical Research: Oceans*, *116*(C12). Retrieved from
929 <https://agupubs.onlinelibrary.wiley.com/doi/abs/10.1029/2011JC006998>
930 doi: <https://doi.org/10.1029/2011JC006998>
- 931 Manizza, M., Menemenlis, D., Zhang, H., & Miller, C. E. (2019). Modeling the re-
932 cent changes in the arctic ocean co2 sink (2006–2013). *Global Biogeochemical Cy-*
933 *cles*, *33*(3), 420–438.
- 934 Mathis, M., Lacroix, F., Hagemann, S., Nielsen, D. M., Ilyina, T., & Schrum, C.
935 (2024). Enhanced co2 uptake of the coastal ocean is dominated by biological
936 carbon fixation. *Nature Climate Change*, 1–7.
- 937 Mathis, M., Logemann, K., Maerz, J., Lacroix, F., Hagemann, S., Chegini, F., ...
938 Schrum, C. (2022). Seamless integration of the coastal ocean in global marine
939 carbon cycle modeling. *Journal of Advances in Modeling Earth Systems*, *14*(8),
940 e2021MS002789.
- 941 Mayorga, E., Seitzinger, S. P., Harrison, J. A., Dumont, E., Beusen, A. H., Bouw-
942 man, A., ... Van Drecht, G. (2010). Global nutrient export from watersheds 2

- (news 2): model development and implementation. *Environmental Modelling & Software*, 25(7), 837–853.
- Medeiros, P. M., Seidel, M., Ward, N. D., Carpenter, E. J., Gomes, H. R., Niggemann, J., ... Dittmar, T. (2015). Fate of the amazon river dissolved organic matter in the tropical atlantic ocean. *Global Biogeochemical Cycles*, 29(5), 677–690.
- Menemenlis, D., Fukumori, I., & Lee, T. (2005). Using green's functions to calibrate an ocean general circulation model. *Monthly weather review*, 133(5), 1224–1240.
- Meybeck, M., & Vörösmarty, C. (1999). Global transfer of carbon by rivers. *Global Change Newsletter*, 37, 18–19.
- Michael Beman, J., Arrigo, K. R., & Matson, P. A. (2005). Agricultural runoff fuels large phytoplankton blooms in vulnerable areas of the ocean. *Nature*, 434(7030), 211–214.
- Middelburg, J. J., Soetaert, K., & Hagens, M. (2020). Ocean alkalinity, buffering and biogeochemical processes. *Reviews of Geophysics*, 58(3), e2019RG000681. Retrieved from <https://agupubs.onlinelibrary.wiley.com/doi/abs/10.1029/2019RG000681> (e2019RG000681 2019RG000681) doi: <https://doi.org/10.1029/2019RG000681>
- Mol, J., Thomas, H., Myers, P. G., Hu, X., & Mucci, A. (2018). Inorganic carbon fluxes on the mackenzie shelf of the beaufort sea. *Biogeosciences*, 15(4), 1011–1027.
- Monteith, D. T., Stoddard, J. L., Evans, C. D., De Wit, H. A., Forsius, M., Høgåsen, T., ... others (2007). Dissolved organic carbon trends resulting from changes in atmospheric deposition chemistry. *Nature*, 450(7169), 537–540.
- Mortenson, E., Steiner, N., Monahan, A. H., Hayashida, H., Sou, T., & Shao, A. (2020). Modeled impacts of sea ice exchange processes on arctic ocean carbon uptake and acidification (1980–2015). *Journal of Geophysical Research: Oceans*, 125(7), e2019JC015782. Retrieved from <https://agupubs.onlinelibrary.wiley.com/doi/abs/10.1029/2019JC015782> (e2019JC015782 10.1029/2019JC015782) doi: <https://doi.org/10.1029/2019JC015782>
- Nakhavali, M. A., Lauerwald, R., Regnier, P., & Friedlingstein, P. (2024). Historical trends and drivers of the laterally transported terrestrial dissolved organic carbon to river systems. *Science of The Total Environment*, 917, 170560. Retrieved from <https://www.sciencedirect.com/science/article/pii/S0048969724006971> doi: <https://doi.org/10.1016/j.scitotenv.2024.170560>
- Nishina, K., Ito, A., Zhou, F., Yan, X., Hayashi, S., & Winiwarter, W. (2021, aug). Historical trends of riverine nitrogen loading from land to the east china sea: a model-based evaluation. *Environmental Research Communications*, 3(8), 085005. Retrieved from <https://dx.doi.org/10.1088/2515-7620/ac1ce8> doi: 10.1088/2515-7620/ac1ce8
- Patra, P. K., Canadell, J. G., Houghton, R. A., Piao, S. L., Oh, N.-H., Ciais, P., ... Lasco, R. (2013). The carbon budget of south asia. *Biogeosciences*, 10(1), 513–527. Retrieved from <https://bg.copernicus.org/articles/10/513/2013/> doi: 10.5194/bg-10-513-2013
- Piao, S. L., Ito, A., Li, S. G., Huang, Y., Ciais, P., Wang, X. H., ... Zhu, B. (2012). The carbon budget of terrestrial ecosystems in east asia over the last two decades. *Biogeosciences*, 9(9), 3571–3586. Retrieved from <https://bg.copernicus.org/articles/9/3571/2012/> doi: 10.5194/bg-9-3571-2012
- Probst, J.-L., Mortatti, J., & Tardy, Y. (1994). Carbon river fluxes and weathering co2 consumption in the congo and amazon river basins. *Applied Geochemistry*, 9(1), 1–13.
- Raymond, P. A., Oh, N.-H., Turner, R. E., & Broussard, W. (2008). Anthropogenically enhanced fluxes of water and carbon from the mississippi river. *Nature*, 451(7177), 449–452.

- 997 Regnier, P., Friedlingstein, P., Ciais, P., Mackenzie, F. T., Gruber, N., Janssens,
998 I. A., ... others (2013). Anthropogenic perturbation of the carbon fluxes from
999 land to ocean. *Nature geoscience*, 6(8), 597–607.
- 1000 Regnier, P., Resplandy, L., Najjar, R. G., & Ciais, P. (2022). The land-to-ocean
1001 loops of the global carbon cycle. *Nature*, 603(7901), 401–410.
- 1002 Resplandy, L., Keeling, R., Rödenbeck, C., Stephens, B., Khatiwala, S., Rodgers, K.,
1003 ... Tans, P. (2018). Revision of global carbon fluxes based on a reassessment of
1004 oceanic and riverine carbon transport. *Nature Geoscience*, 11(7), 504–509.
- 1005 Riquetti, N. B., Beskow, S., Guo, L., & Mello, C. R. (2023). Soil erosion assess-
1006 ment in the amazon basin in the last 60 years of deforestation. *Environmental*
1007 *Research*, 236, 116846. Retrieved from <https://www.sciencedirect.com/science/article/pii/S001393512301650X> doi: <https://doi.org/10.1016/j.envres.2023.116846>
- 1010 Robertson, G. P., & Rosswall, T. (1986). Nitrogen in west africa: the regional cycle.
1011 *Ecological Monographs*, 56(1), 43–72.
- 1012 Rödenbeck, C. (2005). Estimating CO₂ sources and sinks from atmospheric mix-
1013 ing ratio measurements using a global inversion of atmospheric transport. *Techni-
1014 cal reports*.
- 1015 Rödenbeck, C., Keeling, R. F., Bakker, D. C. E., Metzl, N., Olsen, A., Sabine, C., &
1016 Heimann, M. (2013). Global surface-ocean pCO₂ and sea-air CO₂ flux variabil-
1017 ity from an observation-driven ocean mixed-layer scheme. *Ocean Science*, 9(2),
1018 193–216.
- 1019 Samanta, S., Dalai, T. K., Pattanaik, J. K., Rai, S. K., & Mazumdar, A. (2015).
1020 Dissolved inorganic carbon (DIC) and its $\delta^{13}\text{C}$ in the Ganga (Hooghly) River
1021 estuary, India: Evidence of DIC generation via organic carbon degradation
1022 and carbonate dissolution. *Geochimica et Cosmochimica Acta*, 165, 226–248.
1023 Retrieved from <https://www.sciencedirect.com/science/article/pii/S0016703715003658> doi: <https://doi.org/10.1016/j.gca.2015.05.040>
- 1025 Savenko, V. S., & Savenko, A. V. (2021). The main features of phosphorus transport
1026 in world rivers. *Water*, 14(1), 16.
- 1027 Seitzinger, S. P., Mayorga, E., Bouwman, A. F., Kroeze, C., Beusen, A. H., Billen,
1028 G., ... others (2010). Global river nutrient export: A scenario analysis of past
1029 and future trends. *Global biogeochemical cycles*, 24(4).
- 1030 Sharples, J., Middelburg, J. J., Fennel, K., & Jickells, T. D. (2017). What propor-
1031 tion of riverine nutrients reaches the open ocean? *Global Biogeochemical Cycles*,
1032 31(1), 39–58.
- 1033 Singh, A., & Ramesh, R. (2011). Contribution of riverine dissolved inorganic nitro-
1034 gen flux to new production in the coastal northern indian ocean: an assessment.
1035 *International Journal of Oceanography*, 2011.
- 1036 Smith, S. V., Swaney, D. P., Talaue-Mcmanus, L., Bartley, J. D., Sandhei, P. T.,
1037 McLAUGHLIN, C. J., ... others (2003). Humans, hydrology, and the distribution
1038 of inorganic nutrient loading to the ocean. *Bioscience*, 53(3), 235–245.
- 1039 Song, C., Wang, G., Mao, T., Huang, K., Sun, X., Hu, Z., ... Raymond, P. A.
1040 (2020). Spatiotemporal variability and sources of dic in permafrost catchments
1041 of the yangtze river source region: Insights from stable carbon isotope and water
1042 chemistry. *Water Resources Research*, 56(1), e2019WR025343. Retrieved from
1043 <https://agupubs.onlinelibrary.wiley.com/doi/abs/10.1029/2019WR025343>
1044 (e2019WR025343 2019WR025343) doi: <https://doi.org/10.1029/2019WR025343>
- 1045 Spencer, R. G. M., Mann, P. J., Dittmar, T., Eglinton, T. I., McIntyre, C., Holmes,
1046 R. M., ... Stubbins, A. (2015). Detecting the signature of permafrost thaw in
1047 arctic rivers. *Geophysical Research Letters*, 42(8), 2830–2835. Retrieved from
1048 <https://agupubs.onlinelibrary.wiley.com/doi/abs/10.1002/2015GL063498>
1049 doi: <https://doi.org/10.1002/2015GL063498>
- 1050 Suchet, P. A., & Probst, J.-L. (1995). A global model for present-day atmo-

- 1051 spheric/soil co₂ consumption by chemical erosion of continental rocks (gem-co₂).
 1052 *Tellus B*, 47(1-2), 273–280.
- 1053 Suzuki, T., Yamazaki, D., Tsujino, H., Komuro, Y., Nakano, H., & Urakawa, S.
 1054 (2018). A dataset of continental river discharge based on jra-55 for use in a global
 1055 ocean circulation model. *Journal of oceanography*, 74, 421–429.
- 1056 Tagliabue, A., Bowie, A. R., Boyd, P. W., Buck, K. N., Johnson, K. S., & Saito,
 1057 M. A. (2017). The integral role of iron in ocean biogeochemistry. *Nature*,
 1058 543(7643), 51–59.
- 1059 Tank, S. E., Raymond, P. A., Striegl, R. G., McClelland, J. W., Holmes, R. M.,
 1060 Fiske, G. J., & Peterson, B. J. (2012). A land-to-ocean perspective on
 1061 the magnitude, source and implication of dic flux from major arctic rivers
 1062 to the arctic ocean. *Global Biogeochemical Cycles*, 26(4). Retrieved from
 1063 <https://agupubs.onlinelibrary.wiley.com/doi/abs/10.1029/2011GB004192>
 1064 doi: <https://doi.org/10.1029/2011GB004192>
- 1065 Terhaar, J., Lauerwald, R., Regnier, P., Gruber, N., & Bopp, L. (2021). Around one
 1066 third of current arctic ocean primary production sustained by rivers and coastal
 1067 erosion. *Nature Communications*, 12(1), 169.
- 1068 Tian, H., Xu, R., Pan, S., Yao, Y., Bian, Z., Cai, W.-J., ... Yang, J. (2020). Long-
 1069 term trajectory of nitrogen loading and delivery from mississippi river basin to
 1070 the gulf of mexico. *Global Biogeochemical Cycles*, 34(5), e2019GB006475. Re-
 1071 trieved from [https://agupubs.onlinelibrary.wiley.com/doi/abs/10.1029/](https://agupubs.onlinelibrary.wiley.com/doi/abs/10.1029/2019GB006475)
 1072 [2019GB006475](https://doi.org/10.1029/2019GB006475) (e2019GB006475 2019GB006475) doi: [https://doi.org/10.1029/](https://doi.org/10.1029/2019GB006475)
 1073 [2019GB006475](https://doi.org/10.1029/2019GB006475)
- 1074 Tian, H., Yao, Y., Li, Y., Shi, H., Pan, S., Najjar, R. G., ... Leung, L. R. (2023).
 1075 Increased terrestrial carbon export and co₂ evasion from global inland waters
 1076 since the preindustrial era. *Global Biogeochemical Cycles*, 37(10), e2023GB007776.
 1077 Retrieved from [https://agupubs.onlinelibrary.wiley.com/doi/abs/10.1029/](https://agupubs.onlinelibrary.wiley.com/doi/abs/10.1029/2023GB007776)
 1078 [2023GB007776](https://doi.org/10.1029/2023GB007776) (e2023GB007776 2023GB007776) doi: [https://doi.org/10.1029/](https://doi.org/10.1029/2023GB007776)
 1079 [2023GB007776](https://doi.org/10.1029/2023GB007776)
- 1080 Tivig, M., Keller, D. P., & Oschlies, A. (2021). Riverine nitrogen supply to the
 1081 global ocean and its limited impact on global marine primary production: a feed-
 1082 back study using an earth system model. *Biogeosciences*, 18(19), 5327–5350.
 1083 Retrieved from <https://bg.copernicus.org/articles/18/5327/2021/> doi:
 1084 [10.5194/bg-18-5327-2021](https://doi.org/10.5194/bg-18-5327-2021)
- 1085 Tsujino, H., Urakawa, S., Nakano, H., Small, R. J., Kim, W. M., Yeager, S. G., ...
 1086 others (2018). Jra-55 based surface dataset for driving ocean–sea-ice models
 1087 (jra55-do). *Ocean Modelling*, 130, 79–139.
- 1088 Vishwakarma, S., Zhang, X., & Mueller, N. D. (2022). Projecting future nitro-
 1089 gen inputs: are we making the right assumptions? *Environmental Research Let-*
 1090 *ters*, 17(5), 054035.
- 1091 Volta, C., Laruelle, G. G., Arndt, S., & Regnier, P. (2016). Linking biogeochemistry
 1092 to hydro-geometrical variability in tidal estuaries: a generic modeling approach.
 1093 *Hydrology and earth system sciences*, 20(3), 991–1030.
- 1094 Vörösmarty, C., Fekete, B. M., Meybeck, M., & Lammers, R. B. (2000). Global
 1095 system of rivers: Its role in organizing continental land mass and defining land-to-
 1096 ocean linkages. *Global Biogeochemical Cycles*, 14(2), 599–621.
- 1097 Wang, F., Wang, Y., Zhang, J., Xu, H., & Wei, X. (2007). Human impact on the
 1098 historical change of co₂ degassing flux in river changjiang. *Geochemical Transac-*
 1099 *tions*, 8, 1–10.
- 1100 Wang, J., Beusen, A. H., Liu, X., Van Dingenen, R., Dentener, F., Yao, Q., ...
 1101 Bouwman, A. F. (2020). Spatially explicit inventory of sources of nitrogen inputs
 1102 to the yellow sea, east china sea, and south china sea for the period 1970–2010.
 1103 *Earth's Future*, 8(10), e2020EF001516.
- 1104 Wanninkhof, R. (1992). Relationship between wind speed and gas exchange over the

- 1105 ocean. *Journal of Geophysical Research: Oceans*, *97*(C5), 7373–7382.
- 1106 Ward, N. D., Megonigal, J. P., Bond-Lamberty, B., Bailey, V. L., Butman, D.,
1107 Canuel, E. A., . . . others (2020). Representing the function and sensitivity of
1108 coastal interfaces in earth system models. *Nature communications*, *11*(1), 2458.
- 1109 Wunsch, C., & Heimbach, P. (2013). Dynamically and kinematically consistent
1110 global ocean circulation and ice state estimates. In *International geophysics*
1111 (Vol. 103, pp. 553–579). Elsevier.
- 1112 Wunsch, C., Heimbach, P., Ponte, R. M., Fukumori, I., & MEMBERS, E.-G. C.
1113 (2009). The global general circulation of the ocean estimated by the ecco-
1114 consortium. *Oceanography*, *22*(2), 88–103.
- 1115 Yang, M., Nelson, F. E., Shiklomanov, N. I., Guo, D., & Wan, G. (2010). Permafrost
1116 degradation and its environmental effects on the tibetan plateau: A review of re-
1117 cent research. *Earth-Science Reviews*, *103*(1-2), 31–44.
- 1118 Zhang, J., Lu, C., Crumpton, W., Jones, C., Tian, H., Villarini, G., . . . Green, D.
1119 (2022). Heavy precipitation impacts on nitrogen loading to the gulf of mexico in
1120 the 21st century: Model projections under future climate scenarios. *Earth's future*,
1121 *10*(4), e2021EF002141.
- 1122 Zhong, G., Li, X., Song, J., Qu, B., Wang, F., Wang, Y., . . . Xing, J. (2022).
1123 The increasing big gap of carbon sink between the western and eastern pa-
1124 cific in the last three decades. *Frontiers in Marine Science*, *9*. Retrieved from
1125 <https://www.frontiersin.org/articles/10.3389/fmars.2022.1088181> doi:
1126 10.3389/fmars.2022.1088181